NASA TN D-113

NASA TN D-113

TECHNICAL NOTE
D-113

ANALYSIS OF THE DYNAMIC LATERAL STABILITY OF A DELTA-WING AIRPLANE WITH FREQUENCY-DEPENDENT STABILITY DERIVATIVES

By Albert E. Brown and Albert A. Schy

Langley Research Center
Langley Field, Va.

NATIONAL AERONAUTICS AND SPACE ADMINISTRATION

WASHINGTON November 1959

1D

NATIONAL AERONAUTICS AND SPACE ADMINISTRATION

TECHNICAL NOTE D-113

ANALYSIS OF THE DYNAMIC LATERAL STABILITY OF A DELTA-WING AIRPLANE WITH FREQUENCY-DEPENDENT STABILITY DERIVATIVES

By Albert E. Brown and Albert A. Schy

SUMMARY

An analytical investigation has been made to determine the effect of frequency-dependent stability derivatives on the lateral stability of a delta-wing airplane for a flight condition where test results had shown large variations of the stability derivatives with frequency over a range of frequencies. Time histories of rolling velocity and angle of sideslip are obtained by using the Fourier transform to solve the lateral equations of motion. In order to illustrate the frequency effects of the stability derivatives, time histories calculated by using constant values for these derivatives are presented for comparison.

The results of the investigation show that the frequency effects of the stability derivatives can cause considerable changes in predicted airplane motions. Moreover, the results indicate that amplitude effects of these derivatives can also be important in calculating airplane responses.

INTRODUCTION

Currently, perturbed motions of airplanes are generally calculated on the assumption of constant aerodynamic coefficients. However, it has long been known that certain unsteady effects, for example, unsteady lift, downwash, and sidewash, produce aerodynamic lags that cause these coefficients to depend on frequency of oscillation. A number of theoretical investigations have treated unsteady effects on longitudinal stability. However, except for limited simplified analyses (for example, ref. 1) little appears to have been done on the corresponding problem for lateral stability. Recently, wind-tunnel tests using dynamic testing facilities (refs. 2 to 4) have provided all the important lateral stability derivatives of a delta-wing model at subsonic speeds under oscillatory conditions and show a large effect of frequency on these derivatives,

particularly at medium and high angles of attack. In reference 2, in a simplified approach to evaluate frequency effects on lateral stability, calculations were made to determine the effects of unsteady sideslip derivatives on Dutch roll characteristics. In this method values of the stability derivatives at the Dutch roll frequency are used to obtain the roots of the frequency-dependent characteristic equation by iteration. The Dutch roll roots thus obtained seem to be a good approximation of the Dutch roll characteristics in the presence of frequency-dependent stability derivatives. However, Dutch roll frequency-evaluated stability derivatives are based on a sustained harmonic oscillation and therefore in the strict sense are only valid at the Dutch roll frequency. When considering response to arbitrary inputs, it is necessary to consider a range of frequencies in order to obtain correct dynamic response characteristics. In particular, the low-frequency characteristics are important in determining the response after the first few seconds. Therefore the frequency dependence of the lateral derivatives at all frequencies should be brought into the response calculations.

L 5 6 1

The object of the present investigation is to present a general method for incorporating frequency effects and to give some indication of the significance of these effects. Oscillatory data on sideslip, roll, and yaw derivatives, presented in references 2 to 4, are used to calculate typical lateral motions of a delta-wing interceptor by Fourier analysis techniques. These motions are then compared to the motions calculated by using zero-frequency or Dutch roll frequency-evaluated stability derivatives. Results of the oscillation tests to obtain lateral stability derivatives have also shown some effects of amplitude of oscillation, particularly for small amplitudes and low frequencies. These effects are not compatible with linear theory, and no rigorous analysis was attempted to include them. However, some discussion of the amplitude effects is presented by using a simplified qualitative approach.

SYMBOLS

The forces and moments are referred to the principal body axes system shown in figure 1.

b wing span, ft

C_L lift coefficient, $\frac{\text{Lift}}{\frac{1}{2}\rho V^2 S}$

C_l rolling-moment coefficient, $\frac{\text{Rolling moment}}{\frac{1}{2}\rho V^2 S b}$

$$C_{l_\beta} = \frac{\partial C_l}{\partial \beta}$$

$$C_{l_{\dot{\beta}}} = \frac{\partial C_l}{\partial \frac{\dot{\beta} b}{2V}}$$

$$C_{l_p} = \frac{\partial C_l}{\partial \frac{pb}{2V}}$$

$$C_{l_{\dot{p}}} = \frac{\partial C_l}{\partial \frac{\dot{p} b^2}{4V^2}}$$

$$C_{l_r} = \frac{\partial C_l}{\partial \frac{rb}{2V}}$$

$$C_{l_{\dot{r}}} = \frac{\partial C_l}{\partial \frac{\dot{r} b^2}{4V^2}}$$

C_n yawing-moment coefficient, $\frac{\text{Yawing moment}}{\frac{1}{2}\rho V^2 S b}$

$$C_{n_\beta} = \frac{\partial C_n}{\partial \beta}$$

$$C_{n_{\dot{\beta}}} = \frac{\partial C_n}{\partial \frac{\dot{\beta} b}{2V}}$$

$$C_{n_p} = \frac{\partial C_n}{\partial \frac{pb}{2V}}$$

$$C_{n_{\dot{p}}} = \frac{\partial C_n}{\partial \frac{\dot{p} b^2}{4V^2}}$$

$C_{n_r} = \frac{\partial C_n}{\partial \frac{rb}{2V}}$

$C_{n_{\dot{r}}} = \frac{\partial C_n}{\partial \frac{\dot{r}b^2}{4V^2}}$

C_Y lateral-force coefficient, $\frac{\text{Lateral force}}{\frac{1}{2}\rho V^2 S}$

$C_{Y_\beta} = \frac{\partial C_Y}{\partial \beta}$

D differential operator, d/ds

g acceleration due to gravity, ft/sec^2

h altitude, ft

K_{X_o} radius of gyration about principal longitudinal axis, nondimensionalized with respect to b

K_{Z_o} radius of gyration about principal vertical axis, nondimensionalized with respect to b

k reduced-frequency parameter, $\omega b/2V$

m mass of airplane, W/g, slugs

N,n integers

P period of oscillation, sec

p rolling angular velocity, radians/sec except where noted in figures

$\bar{p}$ nondimensional Laplace transform variable $f(\bar{p}) = \int_0^\infty e^{-\bar{p}s} F(s)ds$

$\dot{p}$ rolling angular acceleration, radians/sec^2

R amplitude of complex number

r yawing angular velocity, radians/sec

$\dot{r}$	yawing angular acceleration, radians/sec^2
S	wing area, sq ft
s	nondimensional time parameter based on span, Vt/b
$T_{1/2}$	time for amplitude of oscillation to change by a factor of 2 (positive value indicates a decrease to half amplitude; negative value indicates an increase to double amplitude)
t	time, sec
V	airspeed, ft/sec
W	weight of airplane, lb
α	angle of attack with respect to wing chord plane, deg
β	angle of sideslip, radians except where noted in figures
β_o	amplitude of oscillation, sideslip, deg
$\dot{\beta}$	rate of change of angle of sideslip, radians/sec
ϵ	angle between wing chord plane and principal longitudinal axis, deg (see fig. 1)
η	inclination of principal longitudinal axis with respect to flight path, deg (see fig. 1)
θ	phase of complex number, radians
μ_b	relative density factor, $m/\rho Sb$
ρ	air density, slugs/cu ft
ϕ	angle of roll, radians
ϕ_o	amplitude of oscillation, roll, deg
ψ	angle of yaw, radians
ψ_o	amplitude of oscillation, yaw, deg
ω	angular frequency, radians/sec
$\bar{\omega}$	nondimensional frequency parameter based on span, $\omega b/V$
ω_{DR}	Dutch roll frequency

The symbol s following the subscript of a derivative denotes the derivative referred to the stability system of axes. Square brackets around a ratio of two quantities indicate the transfer function relating the quantities.

ANALYSIS

Preliminary Remarks

The interceptor considered in the present investigation was assumed to have the same lateral stability derivatives as those obtained from the oscillation tests of references 2, 3, and 4. Assumptions of mass and dimensional characteristics reasonable for this delta-wing airplane are given in table I.

Since the experimental oscillatory data showed particularly large effects of frequency for medium and high angles of attack, an angle of attack of 20° was selected for the present investigation for the airplane in level flight at an altitude of 60,000 feet with a velocity of 611 feet per second. Variations of the lateral stability derivatives with reduced frequency parameter are presented in figure 2. The sideslip derivatives were obtained for only one amplitude in reference 2, as shown in figure 2(a), whereas the roll and yaw derivatives of references 3 and 4 (figs. 2(b) and 2(c)) were obtained over a range of amplitudes and showed marked amplitude effects. No data were available on the frequency dependence of side-force derivatives. Because of the relative unimportance of side-force derivatives, it was considered adequate to introduce the most significant C_{Y_β} as a constant and neglect the others. From static tests (ref. 2), $C_{Y_\beta} = -0.52$ at an angle of attack of 20°.

In order to apply linear theory to the calculation of frequency effects, it is necessary to assume that the roll and yaw derivatives are constant with amplitude of oscillation. However, in a simplified attempt to evaluate amplitude effects, results are compared for two sets of stability derivatives which were obtained from test results at two amplitudes of roll oscillation (20° and 5°) and two amplitudes of yaw oscillation (3° and 1.5°). In figures 2(b) and 2(c) the curves representing the frequency-dependent derivatives at larger amplitudes of roll and yaw ($\phi_o = 20°$ and $\psi_o = 3°$) are labeled A and are referred to as "combination A," whereas those at lower amplitudes ($\phi_o = 5°$ and $\psi_o = 1.5°$) are labeled B and are referred to as "combination B." These combinations represent the largest and smallest amplitudes for which test results were available over an adequate frequency range. In order to obtain values

for the derivatives over the frequency range, curves were faired through the test data to the steady-state values of the derivatives.

Variations with reduced frequency parameter of the lateral stability derivatives which were selected for the present investigation are shown in figure 3, converted to the system of principal body axes presented in figure 1.

Equations of Motion

The nondimensionalized linearized lateral equations of motion for level flight, referred to the principal body axes, are as follows:

Rolling:

$$2\mu_b K_{X_o}{}^2 D^2\phi = C_{l_\beta}\beta + \frac{1}{2}C_{l_{\dot{\beta}}}D\beta + \frac{1}{2}C_{l_p}D\phi + \frac{1}{4}C_{l_{\dot{p}}}D^2\phi + \frac{1}{2}C_{l_r}D\psi + \frac{1}{4}C_{l_{\dot{r}}}D^2\psi + C_l \qquad (1a)$$

Yawing:

$$2\mu_b K_{Z_o}{}^2 D^2\psi = C_{n_\beta}\beta + \frac{1}{2}C_{n_{\dot{\beta}}}D\beta + \frac{1}{2}C_{n_r}D\psi + \frac{1}{4}C_{n_{\dot{r}}}D^2\psi + \frac{1}{2}C_{n_p}D\phi + \frac{1}{4}C_{n_{\dot{p}}}D^2\phi + C_n \qquad (1b)$$

Sideslipping:

$$2\mu_b(D\beta + \cos\eta\, D\psi - \sin\eta\, D\phi) = C_{Y_\beta}\beta + \left(C_L \cos\eta\right)\phi + \left(C_L \sin\eta\right)\psi + C_Y \qquad (1c)$$

Solutions of the equations of motion are presented for $D\phi$ and β in response to rolling-and yawing-moment coefficients, since roll rate and sideslip responses are considered to be adequate to describe the lateral dynamic characteristics of the airplane. By use of determinants, the following expressions for the Laplace transforms of the desired solutions were obtained in the usual manner from equations (1):

$$\left.\begin{aligned} \left[\frac{D\phi}{C_l}\right](\bar{p},k) &= \frac{P_1(\bar{p},k)}{Q(\bar{p},k)} & \left[\frac{D\phi}{C_n}\right](\bar{p},k) &= \frac{P_3(\bar{p},k)}{Q(\bar{p},k)} \\ \left[\frac{\beta}{C_l}\right](\bar{p},k) &= \frac{P_2(\bar{p},k)}{Q(\bar{p},k)} & \left[\frac{\beta}{C_n}\right](\bar{p},k) &= \frac{P_4(\bar{p},k)}{Q(\bar{p},k)} \end{aligned}\right\} \qquad (2)$$

where P_1, P_2, P_3, P_4, and Q are polynomials in $\bar{p}$ with coefficients that are functions of reduced-frequency parameter k (because of the dependence of the stability derivatives on k shown in fig. 3). These transfer functions are, of course, simply the ratio of the transform of the output to the transform of the input and are also identical to the transforms of the responses to unit pulse inputs. By simply replacing the Laplace transform variable $\bar{p}$ in these expressions by $i\bar{\omega}$, the Fourier transforms of the transfer functions are obtained. In this form the transfer function is the familiar complex function of the frequency known as the "frequency response" function. It can be written in terms of dimensional frequency ω, nondimensional frequency $\bar{\omega}$, or reduced-frequency parameter k by using the relation $\omega = \frac{V}{b}\bar{\omega} = \frac{2V}{b}k$. L 5 6 1

In terms of k, the desired Fourier transforms are:

$$\left.\begin{aligned}
\left[\frac{D\phi}{C_l}\right](i\bar{\omega},k) &= \frac{P_1(2ik,k)}{Q(2ik,k)} = \frac{\bar{P}_1(k)}{\bar{Q}(k)} \\
\left[\frac{\beta}{C_l}\right](i\bar{\omega},k) &= \frac{P_2(2ik,k)}{Q(2ik,k)} = \frac{\bar{P}_2(k)}{\bar{Q}(k)} \\
\left[\frac{D\phi}{C_n}\right](i\bar{\omega},k) &= \frac{P_3(2ik,k)}{Q(2ik,k)} = \frac{\bar{P}_3(k)}{\bar{Q}(k)} \\
\left[\frac{\beta}{C_n}\right](i\bar{\omega},k) &= \frac{P_4(2ik,k)}{Q(2ik,k)} = \frac{\bar{P}_4(k)}{\bar{Q}(k)}
\end{aligned}\right\} \qquad (3)$$

The complex functions $\bar{P}_1$, $\bar{P}_2$, $\bar{P}_3$, $\bar{P}_4$, and $\bar{Q}$ are presented in appendix A.

Calculations

Frequency-response characteristics and time histories of transient motions in rolling velocity and angle of sideslip were calculated from the transfer functions presented in the preceding section with frequency-dependent and with constant coefficients. The data of table I and $C_{Y_\beta} = -0.520$ are applicable to all calculations. The frequency-dependent solutions were obtained by using the oscillatory sideslip derivatives of

figure 3(a) with large- and with small-amplitude combinations of the oscillatory roll and yaw derivatives from curves A and B of figures 3(b) and 3(c). No attempt was made to express the transfer functions analytically in the frequency-dependent cases. At any desired frequency, values of the transfer functions were simply determined from the values of the derivatives at that frequency. Enough frequency points were used to define adequately the frequency response over the frequency range of interest, which lies between $\omega = 0$ and approximately twice the natural frequency of the lateral oscillation.

The inverse Fourier transform methods and tables of reference 5 were applied to calculate time histories of response to a unit impulse from the frequency-response characteristics of the frequency-dependent transfer functions. By numerical integration of these results, time histories of response to a step input were obtained. In these calculations the procedure of reference 5 was modified to use a varying frequency interval $\Delta\omega$ in the numerical integrations. In many cases the use of varying interval size yields better accuracy with less work, since interval size can be tailored to the slope of the curve. The modified procedure is outlined in an example in appendix B.

For comparison with the frequency-dependent solutions, frequency-independent transfer functions were obtained from the steady-state ($k = 0$) values of the oscillatory stability derivatives and from their values at the Dutch roll frequency. The Dutch roll frequency was obtained by iteration of the frequency-dependent characteristic equation. Corresponding to the large- and small-amplitude combinations of stability derivatives, the Dutch roll oscillation occurred at reduced-frequency parameters of 0.084 and 0.079, respectively. Values of the constant stability derivatives are given in table II, and the solutions of corresponding characteristic equations are presented in table III.

Several significant differences between the characteristics predicted by the steady-state derivatives and those predicted by the derivatives at the Dutch roll frequency are shown by the roots in table III. With regard to Dutch roll period and damping, it can be expected that the results obtained by the iterative method by using values of derivatives at the Dutch roll frequency will be very accurate. Therefore, it is clear that the steady-state derivatives lead to a gross underestimation of the damping and a small overestimation of the period in this case. On the other hand, for the real modes there is no reason to expect the Dutch roll frequency-evaluated derivatives to give accurate answers. Table III shows, for example, that the iterative cases (combinations A and B) predict spiral instability, whereas the steady-state case predicts spiral stability. It is reasonable to assume that the slow spiral mode is better described by the steady-state derivatives and that the unstable spiral roots are incorrect. However, since Fourier techniques are not valid for an unstable system, it was considered necessary

to obtain a direct proof of the stability of the frequency-dependent system. The most convenient way to do this is to check the polar plot of the frequency response in the complex plane (the so-called Nyquist plot). Figure 4 shows a comparison of $\left[D\phi/C_l\right]$ polar plots and indicates that the frequency-dependent system for either combination A or B is stable. Actually, the stable cases (figs. 4(a) and 4(c)) show one clockwise half-encirclement of the origin, but this is caused by the presence of a root with a positive real part in the numerator. The denominator, which is the characteristic equation of the lateral motion, has no unstable roots (as shown in table III) for the steady-state case. There is no encirclement in either unstable case (fig. 4(b)) because the unstable characteristic root (a pole of the transfer function) cancels the effect of the numerator root previously referred to. The frequency responses and time histories calculated for these cases are therefore valid. Comparable time histories for the frequency-independent cases were obtained by the usual Laplace transform method.

L 5 6 1

DISCUSSION OF RESULTS

The frequency-response results are discussed first and then the transient responses are compared. The three cases compared are (a) the case where the stability derivatives are dependent on frequency over the whole significant range from zero to twice the airplane Dutch roll frequency; (b) the case where the stability derivatives are determined at the Dutch roll frequency and (c) the case where the stability derivatives are the steady-state values obtained at zero frequency. Results are shown for frequency-dependent stability derivatives obtained from tests at two levels of oscillation amplitude.

Frequency Responses

Frequency-response characteristics in roll, $\left[D\phi/C_l\right]$ and $\left[D\phi/C_n\right]$, and angle of sideslip, $\left[\beta/C_l\right]$ and $\left[\beta/C_n\right]$, for combination A are presented in figures 5(a), 5(b), 5(c), and 5(d), respectively, and, similarly, for combination B in figures 6(a), 6(b), 6(c), and 6(d), respectively. In these figures, the main differences between the responses obtained with Dutch roll frequency-evaluated (ω_{DR} evaluated) stability derivatives and those obtained with frequency-dependent (ω dependent) derivatives occur at low frequencies. Good agreement is shown near the Dutch roll frequency. As indicated in the results of table III, figures 5 and 6 also show that for the steady-state derivatives the Dutch roll mode is much less damped and occurs at a lower frequency. It is evident from these curves that the steady-state (or pseudostatic)

derivatives (ss-evaluated) give a poor representation of the lateral characteristics. However, the significance of the considerable differences between the Dutch roll frequency-evaluated and frequency-dependent cases in the low-frequency range is not so easy to evaluate. The significance of these differences is best seen in the transient responses, which are discussed in the following section.

It is interesting to note that, in addition to the considerable effects of the frequency-dependent stability derivatives on the frequency responses, there are considerable effects of amplitude of oscillation also. These effects can be seen by comparing the frequency-dependent results of figures 5 and 6 and, to some extent, the iterative roots of table III. Their significance can be seen more clearly by an examination of the transient responses.

Transient Responses

Time histories of rolling velocity and angle of sideslip are presented in figure 7 for a step rolling-moment input and figure 8 for a step yawing-moment input. These figures show a comparison of the motions which would be predicted by using steady-state derivatives, Dutch roll frequency-evaluated derivatives, and frequency-dependent derivatives. A comparison of the results for derivatives obtained for the higher and lower amplitudes of oscillation in the wind-tunnel tests is also shown, but for the purposes of this study the effects of frequency are of primary interest.

The case of the steady-state derivatives can be immediately dismissed, since it shows a Dutch roll oscillation which is much too large and lightly damped. This result merely confirms the fact, which has been pointed out in previous studies, that the pseudostatic derivatives are inadequate for determining the Dutch roll characteristics of highly swept configurations at moderate to high angles of attack. The large amplitude of the oscillations is of particular interest, since it could not be predicted from the characteristic roots alone.

However, the most interesting result shown by the transient motions is the large differences between the Dutch roll frequency-evaluated motions and the frequency-dependent motions, which develop after the first few seconds. These large effects in the predicted responses correspond to the low-frequency discrepancies shown in the frequency-response plots of figures 5 and 6. As mentioned in the discussion of those figures, the importance of these discrepancies was difficult to evaluate without looking at the predicted time histories. The results of figures 7 and 8 seem to indicate that the iterative method of using the Dutch roll frequency-evaluated stability derivatives in the calculation

of the lateral motions of an aircraft can lead to errors whose magnitudes are comparable to those introduced by simply using the steady-state derivatives. These results, of course, apply only to those flight conditions where stability derivatives are strongly dependent on frequency.

Comparison of motions incorporating frequency effects shows appreciable effects of amplitude. The amplitude effects seem to affect the motions as much as the frequency effects, that is, the differences between the frequency-dependent motions for combinations A and B are generally as large as the differences (for a given amplitude combination) between the frequency-dependent and the frequency-independent responses. This result indicates that a complete analysis must take into account amplitude effects. However, for the purpose of the present investigation, the frequency effects are of primary interest, and the results have shown that these can be important in calculating airplane responses. It is recommended that the amplitude effects revealed in the present paper be investigated in a more detailed analysis.

L 5 6 1

CONCLUDING REMARKS

The results of the investigation to determine the effects of frequency-dependent stability derivatives show, for a flight condition where test results had shown large variations of these derivatives with frequency over a range of frequencies, that the frequency effects of the stability derivatives can cause considerable changes in predicted airplane motions. Moreover, the results indicate that amplitude effects of these derivatives can also be important in calculating airplane responses. It is recommended that the amplitude effects revealed in the present paper be investigated in a more detailed analysis.

Langley Research Center,
National Aeronautics and Space Administration,
Langley Field, Va., July 23, 1959.

APPENDIX A

FREQUENCY-RESPONSE FUNCTIONS

The Laplace transform (ref. 6) of the lateral equations of motion (1) for input C_l or C_n yields the following equations for frequency-dependent derivatives such as those plotted in figure 3 as functions of the reduced-frequency parameter k:

$$\left.\begin{aligned}
&\left\{\left[2\mu_b K_{X_o}{}^2 - \tfrac{1}{4}C_{l_{\dot{p}}}(k)\right]\bar{p} - \tfrac{1}{2}C_{l_p}(k)\right\}D\phi(\bar{p}) - \left[\tfrac{1}{4}C_{l_{\dot{r}}}(k)\bar{p} + \tfrac{1}{2}C_{l_r}(k)\right]D\psi(\bar{p}) \\
&-\left[\tfrac{1}{2}C_{l_{\dot{\beta}}}(k)\bar{p} + C_{l_\beta}(k)\right]\beta(\bar{p}) = C_l(\bar{p}) \\
&-\left[\tfrac{1}{4}C_{n_{\dot{p}}}(k)\bar{p} + \tfrac{1}{2}C_{n_p}(k)\right]D\phi(\bar{p}) + \left\{\left[2\mu_b K_{Z_o}{}^2 - \tfrac{1}{4}C_{n_{\dot{r}}}(k)\right]\bar{p} - \tfrac{1}{2}C_{n_r}(k)\right\}D\psi(\bar{p}) \\
&-\left[\tfrac{1}{2}C_{n_{\dot{\beta}}}(k)\bar{p} + C_{n_\beta}(k)\right]\beta(\bar{p}) = C_n(\bar{p}) \\
&-\left(2\mu_b \sin\eta + \frac{C_L\cos\eta}{\bar{p}}\right)D\phi(\bar{p}) + \left(2\mu_b\cos\eta - \frac{C_L\sin\eta}{\bar{p}}\right)D\psi(\bar{p}) \\
&+\left(2\mu_b\bar{p} - C_{Y_\beta}\right)\beta(\bar{p}) = 0
\end{aligned}\right\} \quad \text{(A1)}$$

where $\bar{p}$ is the Laplace transform variable.

By the use of determinants the expressions obtained from equations (A1) for $\frac{D\phi}{C_l}$, $\frac{\beta}{C_l}$, $\frac{D\phi}{C_n}$, and $\frac{\beta}{C_n}$ are as follows:

$$\left.\begin{aligned}
\left[\frac{D\phi}{C_l}\right](\bar{p},k) &= \frac{A_1\bar{p}^3 + B_1\bar{p}^2 + C_1\bar{p} + D_1}{A\bar{p}^4 + B\bar{p}^3 + C\bar{p}^2 + D\bar{p} + E} \\
\left[\frac{\beta}{C_l}\right](\bar{p},k) &= \frac{A_2\bar{p}^2 + B_2\bar{p} + C_2}{A\bar{p}^4 + B\bar{p}^3 + C\bar{p}^2 + D\bar{p} + E} \\
\left[\frac{D\phi}{C_n}\right](\bar{p},k) &= \frac{A_3\bar{p}^3 + B_3\bar{p}^2 + C_3\bar{p} + D_3}{A\bar{p}^4 + B\bar{p}^3 + C\bar{p}^2 + D\bar{p} + E} \\
\left[\frac{\beta}{C_n}\right](\bar{p},k) &= \frac{A_4\bar{p}^2 + B_4\bar{p} + C_4}{A\bar{p}^4 + B\bar{p}^3 + C\bar{p}^2 + D\bar{p} + E}
\end{aligned}\right\} \qquad (A2)$$

Equations (A2) show the polynomials P_1, P_2, P_3, P_4, and Q which appear in equations (2). The coefficients of the polynomials are defined as follows:

$$A = \mu_b{}^2\left[8\mu_b K_{X_o}{}^2 K_{Z_o}{}^2 - K_{X_o}{}^2 C_{n_{\dot{r}}}(k) - K_{Z_o}{}^2 C_{l_{\dot{p}}}(k)\right]$$

$$+ \mu_b\left[\tfrac{1}{8}C_{l_{\dot{p}}}(k)C_{n_{\dot{r}}}(k) - \tfrac{1}{8}C_{l_{\dot{r}}}(k)C_{n_{\dot{p}}}(k)\right]$$

$$B = -2\mu_b{}^2\left[2K_{X_o}{}^2 K_{Z_o}{}^2 C_{Y_\beta} + K_{X_o}{}^2 C_{n_r}(k) + K_{Z_o}{}^2 C_{l_p}(k) + K_{Z_o}{}^2 C_{l_{\dot{\beta}}}(k)\sin\eta\right.$$

$$\left. - K_{X_o}{}^2 C_{n_{\dot{\beta}}}(k)\cos\eta\right] + \mu_b\left[\tfrac{1}{2}K_{X_o}{}^2 C_{Y_\beta} C_{n_{\dot{r}}}(k) + \tfrac{1}{2}K_{Z_o}{}^2 C_{Y_\beta} C_{l_{\dot{p}}}(k)\right.$$

$$+ \tfrac{1}{4}C_{n_r}(k)C_{l_{\dot{p}}}(k) + \tfrac{1}{4}C_{l_p}(k)C_{n_{\dot{r}}}(k) - \tfrac{1}{4}C_{n_p}(k)C_{l_{\dot{r}}}(k) - \tfrac{1}{4}C_{l_r}(k)C_{n_{\dot{p}}}(k)$$

$$- \tfrac{1}{4}C_{n_{\dot{\beta}}}(k)C_{l_{\dot{p}}}(k)\cos\eta + \tfrac{1}{4}C_{l_{\dot{\beta}}}(k)C_{n_{\dot{p}}}(k)\cos\eta - \tfrac{1}{4}C_{n_{\dot{\beta}}}(k)C_{l_{\dot{r}}}(k)\sin\eta$$

$$\left. + \tfrac{1}{4}C_{l_{\dot{\beta}}}(k)C_{n_{\dot{r}}}(k)\sin\eta\right] - \tfrac{1}{16}C_{Y_\beta}C_{l_{\dot{p}}}(k)C_{n_{\dot{r}}}(k) + \tfrac{1}{16}C_{Y_\beta}C_{n_{\dot{p}}}(k)C_{l_{\dot{r}}}(k)$$

$$C = \mu_b\Big[4\mu_b K_{X_o}{}^2 C_{n_\beta}(k)\cos\eta - 4\mu_b K_{Z_o}{}^2 C_{l_\beta}(k)\sin\eta + K_{X_o}{}^2 C_{Y_\beta} C_{n_r}(k)$$

$$+ K_{Z_o}{}^2 C_{Y_\beta} C_{l_p}(k) - K_{X_o}{}^2 C_{n_{\dot\beta}}(k) C_L \sin\eta - K_{Z_o}{}^2 C_{l_{\dot\beta}}(k) C_L \cos\eta$$

$$+ \tfrac{1}{2} C_{n_r}(k) C_{l_p}(k) - \tfrac{1}{2} C_{l_r}(k) C_{n_p}(k) - \tfrac{1}{2} C_{n_\beta}(k) C_{l_{\dot p}}(k)\cos\eta$$

$$- \tfrac{1}{2} C_{n_{\dot\beta}}(k) C_{l_p}(k)\cos\eta - \tfrac{1}{2} C_{n_\beta}(k) C_{l_{\dot r}}(k)\sin\eta - \tfrac{1}{2} C_{n_{\dot\beta}}(k) C_{l_r}(k)\sin\eta$$

$$+ \tfrac{1}{2} C_{l_\beta}(k) C_{n_{\dot p}}(k)\cos\eta + \tfrac{1}{2} C_{l_{\dot\beta}}(k) C_{n_p}(k)\cos\eta + \tfrac{1}{2} C_{l_\beta}(k) C_{n_{\dot r}}(k)\sin\eta$$

$$+ \tfrac{1}{2} C_{l_{\dot\beta}}(k) C_{n_r}(k)\sin\eta\Big] + \tfrac{1}{8}\Big[C_{Y_\beta} C_{n_p}(k) C_{l_{\dot r}}(k) + C_{Y_\beta} C_{l_r}(k) C_{n_{\dot p}}(k)$$

$$- C_{Y_\beta} C_{n_r}(k) C_{l_{\dot p}}(k) - C_{Y_\beta} C_{l_p}(k) C_{n_{\dot r}}(k) + C_{n_{\dot\beta}}(k) C_{l_{\dot p}}(k) C_L \sin\eta$$

$$- C_{l_{\dot\beta}}(k) C_{n_{\dot p}}(k) C_L \sin\eta + C_{l_{\dot\beta}}(k) C_{n_{\dot r}}(k) C_L \cos\eta - C_{n_{\dot\beta}}(k) C_{l_{\dot r}}(k) C_L \cos\eta\Big]$$

$$D = \mu_b\Big[-2K_{X_o}{}^2 C_{n_\beta}(k) C_L \sin\eta - 2K_{Z_o}{}^2 C_{l_\beta}(k) C_L \cos\eta + C_{l_\beta}(k) C_{n_r}(k)\sin\eta$$

$$- C_{n_\beta}(k) C_{l_r}(k)\sin\eta + C_{l_\beta}(k) C_{n_p}(k)\cos\eta - C_{n_\beta}(k) C_{l_p}(k)\cos\eta\Big]$$

$$+ \tfrac{1}{4}\Big[C_{Y_\beta} C_{n_p}(k) C_{l_r}(k) - C_{Y_\beta} C_{n_r}(k) C_{l_p}(k) + C_{n_{\dot\beta}}(k) C_{l_p}(k) C_L \sin\eta$$

$$+ C_{n_\beta}(k) C_{l_{\dot p}}(k) C_L \sin\eta - C_{l_\beta}(k) C_{n_{\dot p}}(k) C_L \sin\eta - C_{l_{\dot\beta}}(k) C_{n_p}(k) C_L \sin\eta$$

$$+ C_{l_\beta}(k) C_{n_{\dot r}}(k) C_L \cos\eta + C_{l_{\dot\beta}}(k) C_{n_r}(k) C_L \cos\eta$$

$$- C_{n_{\dot\beta}}(k) C_{l_r}(k) C_L \cos\eta - C_{n_\beta}(k) C_{l_{\dot r}}(k) C_L \cos\eta\Big]$$

$$E = \tfrac{1}{2} C_L\Big[C_{l_p}(k) C_{n_\beta}(k) - C_{n_p}(k) C_{l_\beta}(k)\Big]\sin\eta + \tfrac{1}{2} C_L\Big[C_{n_r}(k) C_{l_\beta}(k) - C_{l_r}(k) C_{n_\beta}(k)\Big]\cos\eta$$

$$A_1 = \mu_b\left[4\mu_b K_{Z_o}{}^2 - \tfrac{1}{2}C_{n_{\dot{r}}}(k)\right]$$

$$B_1 = \mu_b\left[C_{n_{\dot{\beta}}}(k)\cos\eta - C_{n_r}(k) - 2K_{Z_o}{}^2 C_{Y_\beta}\right] + \tfrac{1}{4}C_{Y_\beta}C_{n_{\dot{r}}}(k)$$

$$C_1 = 2\mu_b C_{n_\beta}(k)\cos\eta + \tfrac{1}{2}C_{Y_\beta}C_{n_r}(k) - \tfrac{1}{2}C_{n_{\dot{\beta}}}(k)C_L\sin\eta$$

$$D_1 = -C_{n_\beta}(k)C_L\sin\eta$$

$$A_2 = \mu_b\left[4\mu_b K_{Z_o}{}^2\sin\eta - \tfrac{1}{2}C_{n_{\dot{p}}}(k)\cos\eta - \tfrac{1}{2}C_{n_{\dot{r}}}(k)\sin\eta\right]$$

$$B_2 = \mu_b\left[2K_{Z_o}{}^2 C_L\cos\eta - C_{n_p}(k)\cos\eta - C_{n_r}(k)\sin\eta\right]$$

$$+ \tfrac{1}{4}C_{n_{\dot{p}}}(k)C_L\sin\eta - \tfrac{1}{4}C_{n_{\dot{r}}}(k)C_L\cos\eta$$

$$C_2 = \tfrac{1}{2}C_{n_p}(k)C_L\sin\eta - \tfrac{1}{2}C_{n_r}(k)C_L\cos\eta$$

$$A_3 = \tfrac{1}{2}\mu_b C_{l_{\dot{r}}}(k)$$

$$B_3 = \mu_b\left[C_{l_r}(k) - C_{l_{\dot{\beta}}}(k)\cos\eta\right] - \tfrac{1}{4}C_{Y_\beta}C_{l_{\dot{r}}}(k)$$

$$C_3 = -2\mu_b C_{l_\beta}(k)\cos\eta + \tfrac{1}{2}C_{l_{\dot{\beta}}}(k)C_L\sin\eta - \tfrac{1}{2}C_{Y_\beta}C_{l_r}(k)$$

$$D_3 = C_{l_\beta}(k)C_L\sin\eta$$

L
5
6
1

$$A_4 = \mu_b \left[4\mu_b K_{X_o}^2 \cos\eta + \tfrac{1}{2} C_{l_p}(k)\cos\eta + \tfrac{1}{2} C_{l_{\dot{r}}}(k)\sin\eta \right]$$

$$B_4 = \mu_b \left[2K_{X_o}{}^2 C_L \sin\eta + C_{l_r}(k)\sin\eta + C_{l_p}(k)\cos\eta \right] + \tfrac{1}{4} C_{l_{\dot{r}}}(k) C_L \cos\eta - \tfrac{1}{4} C_{l_{\dot{p}}}(k) C_L \sin\eta$$

$$C_4 = \tfrac{1}{2} C_{l_r}(k) C_L \cos\eta - \tfrac{1}{2} C_{l_p}(k) C_L \sin\eta$$

L
5
6
1

Replacing the Laplace transform variable by $2ik$ in equations (A2) yields the expressions for the polynomials in k of equations (3) as follows:

$$\left.\begin{aligned}
\left[\frac{D\phi}{C_l}\right] &= \frac{\bar{P}_1}{\bar{Q}} = \frac{\bar{B}_1 k^2 + \bar{D}_1 + i\left(\bar{A}_1 k^3 + \bar{C}_1 k\right)}{\bar{A}k^4 + \bar{C}k^2 + \bar{E} + i\left(\bar{B}k^3 + \bar{D}k\right)} \\
\left[\frac{\beta}{C_l}\right] &= \frac{\bar{P}_2}{\bar{Q}} = \frac{\bar{A}_2 k^2 + \bar{C}_2 + i\bar{B}_2 k}{\bar{A}k^4 + \bar{C}k^2 + \bar{E} + i\left(\bar{B}k^3 + \bar{D}k\right)} \\
\left[\frac{D\phi}{C_n}\right] &= \frac{\bar{P}_3}{\bar{Q}} = \frac{\bar{B}_3 k^2 + \bar{D}_3 + i\left(\bar{A}_3 k^3 + \bar{C}_3 k\right)}{\bar{A}k^4 + \bar{C}k^2 + \bar{E} + i\left(\bar{B}k^3 + \bar{D}k\right)} \\
\left[\frac{\beta}{C_n}\right] &= \frac{\bar{P}_4}{\bar{Q}} = \frac{\bar{A}_4 k^2 + \bar{C}_4 + i\bar{B}_4 k}{\bar{A}k^4 + \bar{C}k^2 + \bar{E} + i\left(\bar{B}k^3 + \bar{D}k\right)}
\end{aligned}\right\} \qquad (A3)$$

where in terms of the coefficients of equations (A2)

$$\bar{A} = 16A \qquad \bar{B} = -8B \qquad \bar{C} = -4C \qquad \bar{D} = 2D \qquad \bar{E} = E$$

$$\bar{A}_1 = -8A_1 \qquad \bar{B}_1 = -4B_1 \qquad \bar{C}_1 = 2C_1 \qquad \bar{D}_1 = D_1$$

$$\bar{A}_2 = -4A_2 \qquad \bar{B}_2 = 2B_2 \qquad \bar{C}_2 = C_2$$

$$\bar{A}_3 = -8A_3 \qquad \bar{B}_3 = -4B_3 \qquad \bar{C}_3 = 2C_3 \qquad \bar{D}_3 = D_3$$

$$\bar{A}_4 = -4A_4 \qquad \bar{B}_4 = 2B_4 \qquad \bar{C}_4 = C_4$$

APPENDIX B

ILLUSTRATIVE EXAMPLE OF THE USE OF UNEQUAL FREQUENCY INTERVALS FOR DETERMINING THE TIME RESPONSE TO A UNIT IMPULSE FROM FREQUENCY-RESPONSE DATA

The present investigation suggests a modification to use unequal frequency intervals in the procedure of reference 5 for determining the time response to a unit impulse from frequency-response data. In the modified procedure the choice of frequency intervals used in the stepwise representation of the real component of the frequency response is made on the basis of the local shape of this curve. Where the rate of change of the curve is large, small intervals are used to get a satisfactory fit of the curve, and where the rate of change is smaller, larger intervals may be used. In this way, a good fit for the curve may be obtained, with correspondingly good accuracy in the calculated impulse response, by using considerably fewer intervals than with constant intervals, since then the interval size must be chosen uniformly small to fit the most rapid variations of the curve. When it is desired to introduce a new frequency interval in the stepwise representation the only condition that needs to be satisfied is that the value of frequency at which the new frequency interval is introduced must be an integer multiple of this frequency interval. The following summation, from equation (8) of reference 5, has been shown to be a convenient numerical representation of the integral which defines the impulse response in terms of the real part of the frequency response:

$$f(t) = \frac{2}{\pi} \Delta\omega \sum_{n=1}^{N} r_n \left[\frac{\sin z \cos(2n - 1)z}{z} \right]$$

Here $z = \frac{\Delta\omega}{2} t$, and r_n is the value of the stepwise representation of the real part of the frequency response in the nth frequency interval. The function in brackets is tabulated in reference 5 for a large range of values of n and z. The notation $n = N$ has been changed from that of reference 5, $n = \infty$, because in practice the summation goes to a finite number when the real part r_n becomes negligible. When unequal frequency intervals are used, the summation shown above simply becomes a sum of summations as shown in the example that follows. For illustration, the modified procedure has been applied to the lightly damped roll rate response obtained with the steady-state-evaluated derivatives, which is

defined by the following transfer function:

$$\left[\frac{D\phi}{C_l}\right](\bar{p}) = \frac{8109\bar{p}^3 + 60.56\bar{p}^2 + 37.78\bar{p} - 0.0413}{26543\bar{p}^4 + 823.8\bar{p}^3 + 534.7\bar{p}^2 + 10.53\bar{p} + 0.0159}$$

As shown in figure 9, frequency intervals of 0.10, 0.25, and 0.50 radian per second, $\Delta\omega_1$, $\Delta\omega_2$, and $\Delta\omega_3$, respectively, were chosen for the stepwise representation of the real component of the frequency response. The time response was then readily calculated from the following expression:

$$F(t) = \frac{2}{\pi}\Delta\omega_1 \sum_{n=21}^{n=25} \frac{\sin z_1 \cos(2n-1)z_1}{z_1} + \frac{2}{\pi}\Delta\omega_2 \sum_{n=1}^{n=2} \frac{\sin z_2 \cos(2n-1)z_2}{z_2}$$

$$+ \frac{2}{\pi}\Delta\omega_3 \left[\sum_{n=2}^{n=4} \frac{\sin z_3 \cos(2n-1)z_3}{z_3} + \sum_{n=6}^{n=10} \frac{\sin z_3 \cos(2n-1)z_3}{z_3}\right]$$

where $z_1 = \frac{\Delta\omega_1}{2}t$, $z_2 = \frac{\Delta\omega_2}{2}t$, and $z_3 = \frac{\Delta\omega_3}{2}t$

For comparison results were also obtained with a frequency interval of 0.25 radian per second throughout the frequency range. In figure 9 comparison of the time responses obtained by numerical integration with the exact response obtained analytically shows that the response obtained with three frequency intervals is in much better agreement with the exact response. It is to be noted that this response was obtained from 15 values of amplitude whereas 20 values were used to obtain the response with the constant frequency interval.

REFERENCES

1. Goland, Martin, Hager, Richard G., and Luke, Yudell L.: Aerodynamic Lag in Lateral Control-Free Dynamic Stability (Including a Method for Its Inclusion in Design.) WADC Tech. Rep. 54-259, U. S. Air Force, May 1954.

2. Lichtenstein, Jacob H., and Williams, James L.: Effect of Frequency of Sideslipping Motion on the Lateral Stability Derivatives of a Typical Delta-Wing Airplane. NACA RM L57F07, 1957.

3. Fisher, Lewis R.: Experimental Determination of the Effects of Frequency and Amplitude of Oscillation on the Roll-Stability Derivatives for a 60° Delta-Wing Airplane Model. NACA RM L57L17, 1958.

4. Letko, William, and Fletcher, Herman S.: Effects of Frequency and Amplitude on the Yawing Derivatives of Triangular, Swept, and Unswept Wings and of a Triangular-Wing—Fuselage Combination With and Without a Triangular Tail Performing Sinusoidal Yawing Oscillations. NACA TN 4390, 1958.

5. Huss, Carl R., and Donegan, James J.: Tables for the Numerical Determination of the Fourier Transform of a Function of Time and the Inverse Fourier Transform of a Function of Frequency, With Some Applications to Operational Calculus Methods. NACA TN 4073, 1957.

6. Churchill, Ruel V.: Modern Operational Mathematics in Engineering. McGraw-Hill Book Co., Inc., 1944.

TABLE I.- DIMENSIONAL AND MASS CHARACTERISTICS

ASSUMED FOR AIRPLANE

Weight, lb	24,811
g, ft/sec^2	32
$(\mu_b)_{h=60,000}$	136.38
V, ft/sec	611
$K_{X_o}{}^2$	0.012
$K_{Z_o}{}^2$	0.109
ϵ, deg	1.2
Wing:	
Area, sq ft	652
Span, ft	38.8
Aspect ratio	2.18
Sweepback of leading edge, deg	60
Vertical tail:	
Area, sq ft	116
Span, ft	15.9
Aspect ratio	2.18
Sweepback of leading edge, deg	42.5

TABLE II.- VALUES FOR ALL CONSTANT LATERAL DERIVATIVES USED IN STABILITY CALCULATIONS

[Values are referred to the system of principal body axes]

Combination	k	C_{l_β}	C_{n_β}	C_{Y_β}	C_{l_p}	C_{n_p}	C_{l_r}	C_{n_r}	$C_{l_{\dot\beta}}$	$C_{n_{\dot\beta}}$	$C_{l_{\dot p}}$	$C_{n_{\dot p}}$	$C_{l_{\dot r}}$	$C_{n_{\dot r}}$
Steady-state combination	0	-0.153	0.138	-0.520	-0.154	-0.075	0.035	-0.331	0	0	0	0	0	0
Combination A	.084	-.165	.225	-.520	-.263	-.076	.489	-.322	-.349	-.154	1.880	-.932	-3.695	7.730
Combination B	.079	-.163	.225	-.520	-.222	.066	.627	-.731	-.353	-.141	.754	-.135	-2.042	4.402

TABLE III.- CALCULATION CONDITIONS AND CHARACTERISTIC RESULTS FOR FREQUENCY-INDEPENDENT TRANSFER FUNCTIONS

[h = 60,000 ft; C_L = 0.912; η = 18.8°; μ_b = 136.38; $K_{X_o}{}^2$ = 0.012; $K_{Z_o}{}^2$ = 0.109; V = 611 ft/sec]

Lateral stability derivatives		Results				
Combination	Conditions	Nondimensional roots	Aperiodic modes		Oscillatory modes	
			$T_{1/2}$, sec	$T_{1/2}$, sec	P, sec	$T_{1/2}$, sec
Steady state	Constants at k = 0	-0.00165 -0.0183 -0.00554 ± 0.1411i	26.66	2.41	2.83	7.94
A	Constants at k = 0.084	+0.00277 -0.0217 -0.0270 ± 0.1671i	-15.88	2.03	2.38	1.63
B	Constants at k = 0.079	+0.00163 -0.0155 -0.0266 ± 0.1581i	-27.02	2.83	2.52	1.65

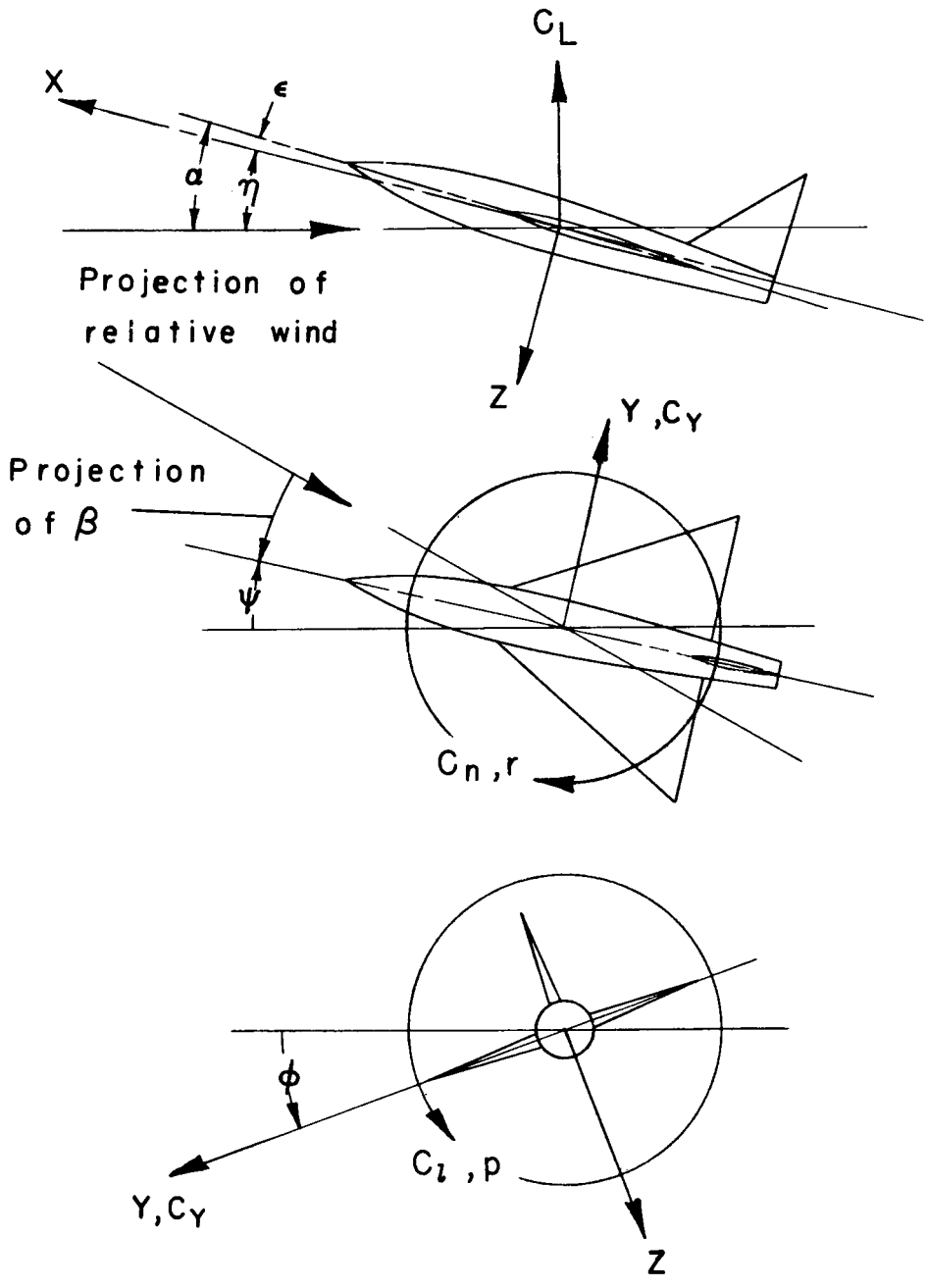

Figure 1.- Sketch showing principal body axes system. Each view presents a plane of the axis system as viewed along the third axis. Positive values of forces, moments, and angles are indicated by arrows.

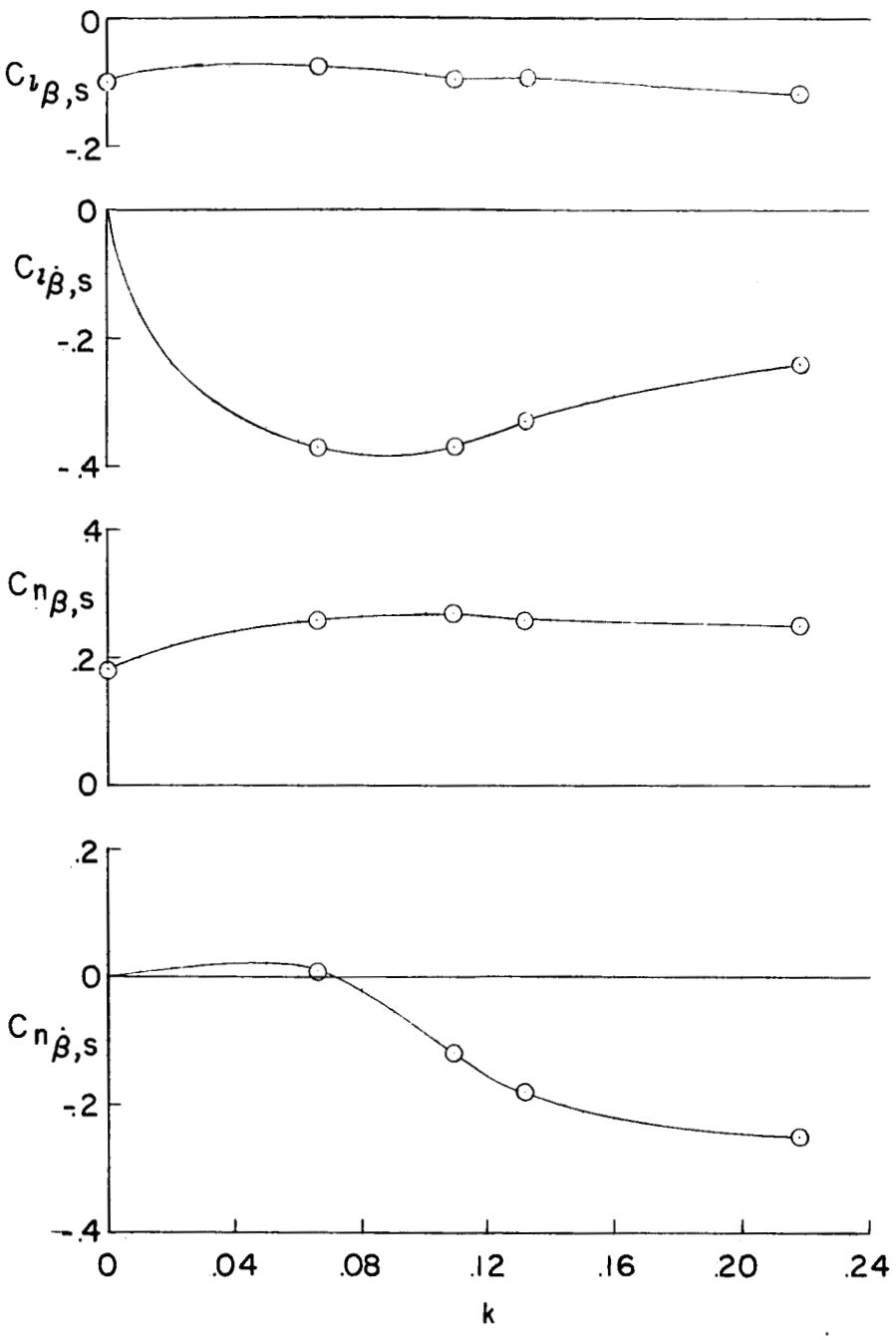

(a) Sideslip derivatives; $\beta_o = \pm 2^\circ$.

Figure 2.- Variations of lateral stability derivatives with reduced-frequency parameter for an angle of attack of 20°.

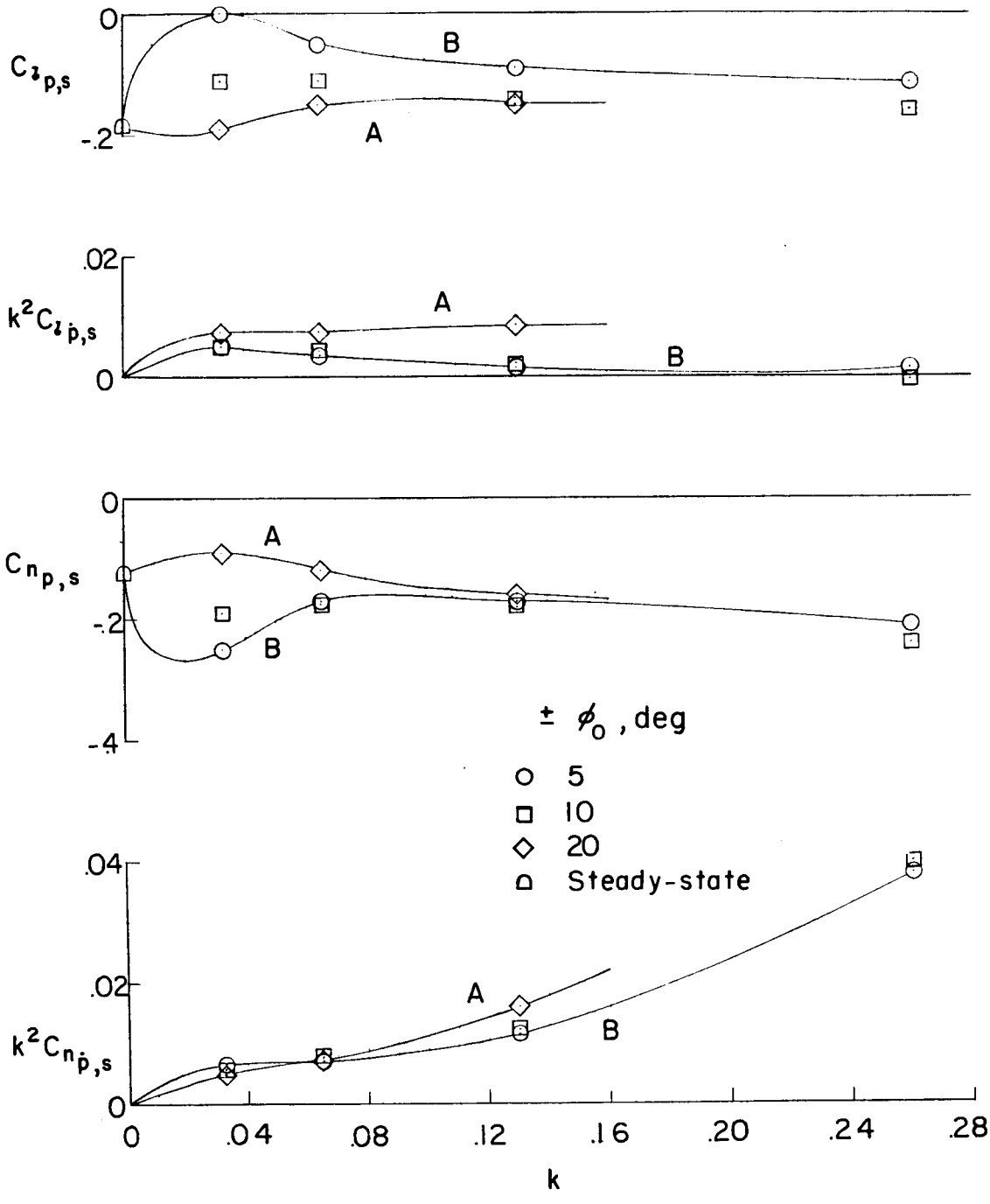

(b) Roll derivatives, including amplitude effects.

Figure 2.- Continued.

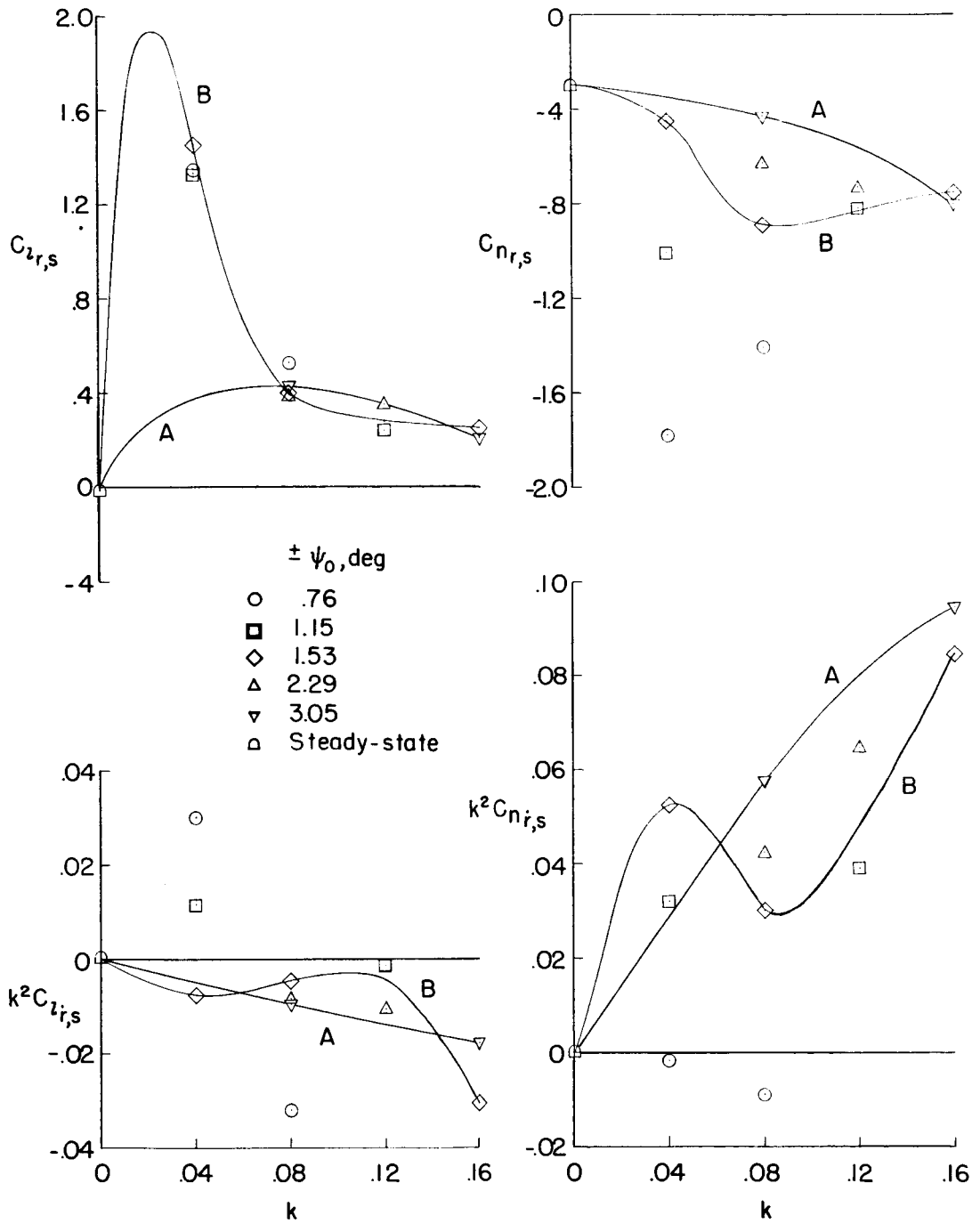

(c) Yaw derivatives, including amplitude effects.

Figure 2.- Concluded.

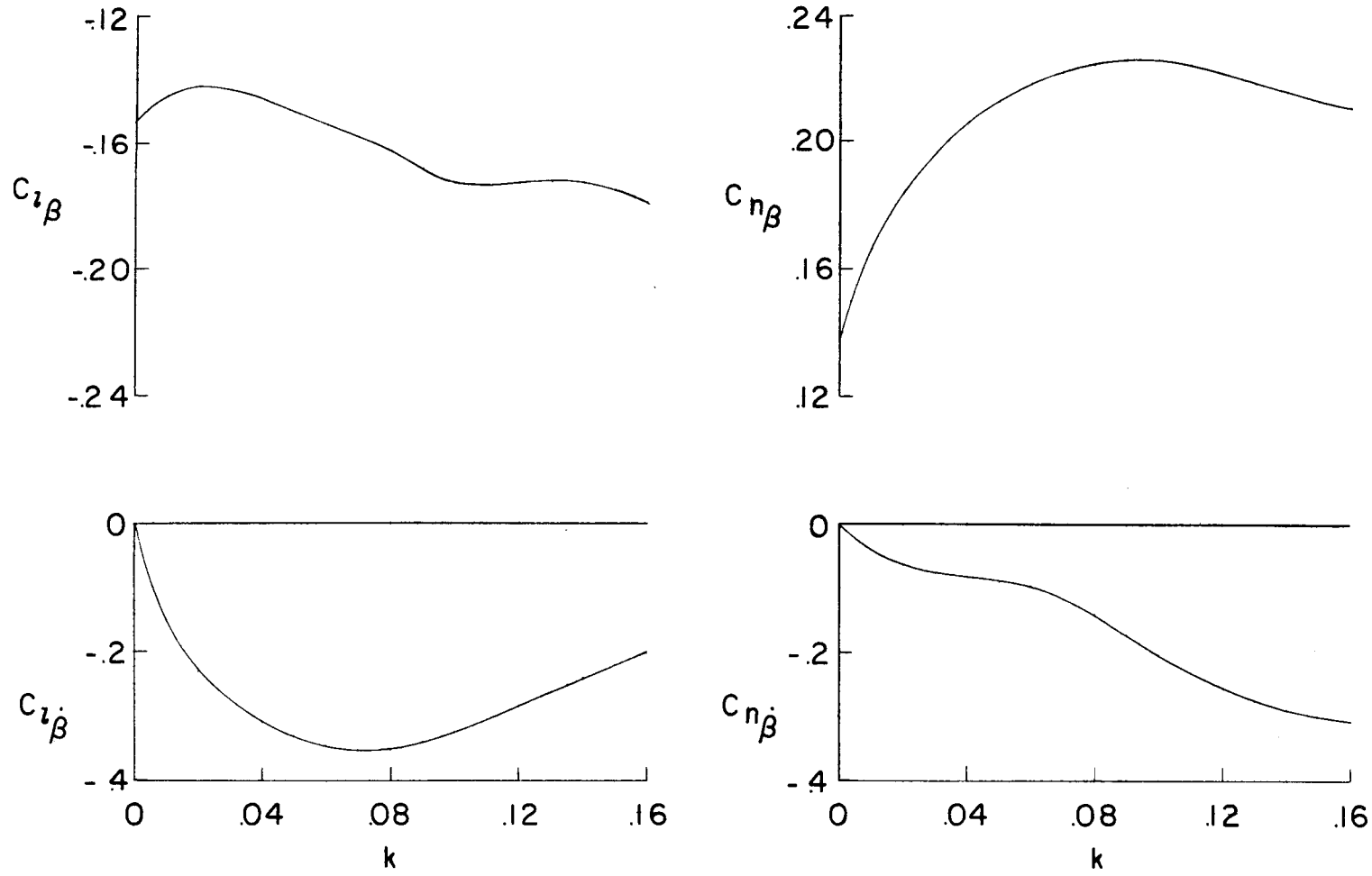

(a) Sideslip derivatives.

Figure 3.- Variations of lateral stability derivatives with reduced-frequency parameter transformed to the system of principal body axes.

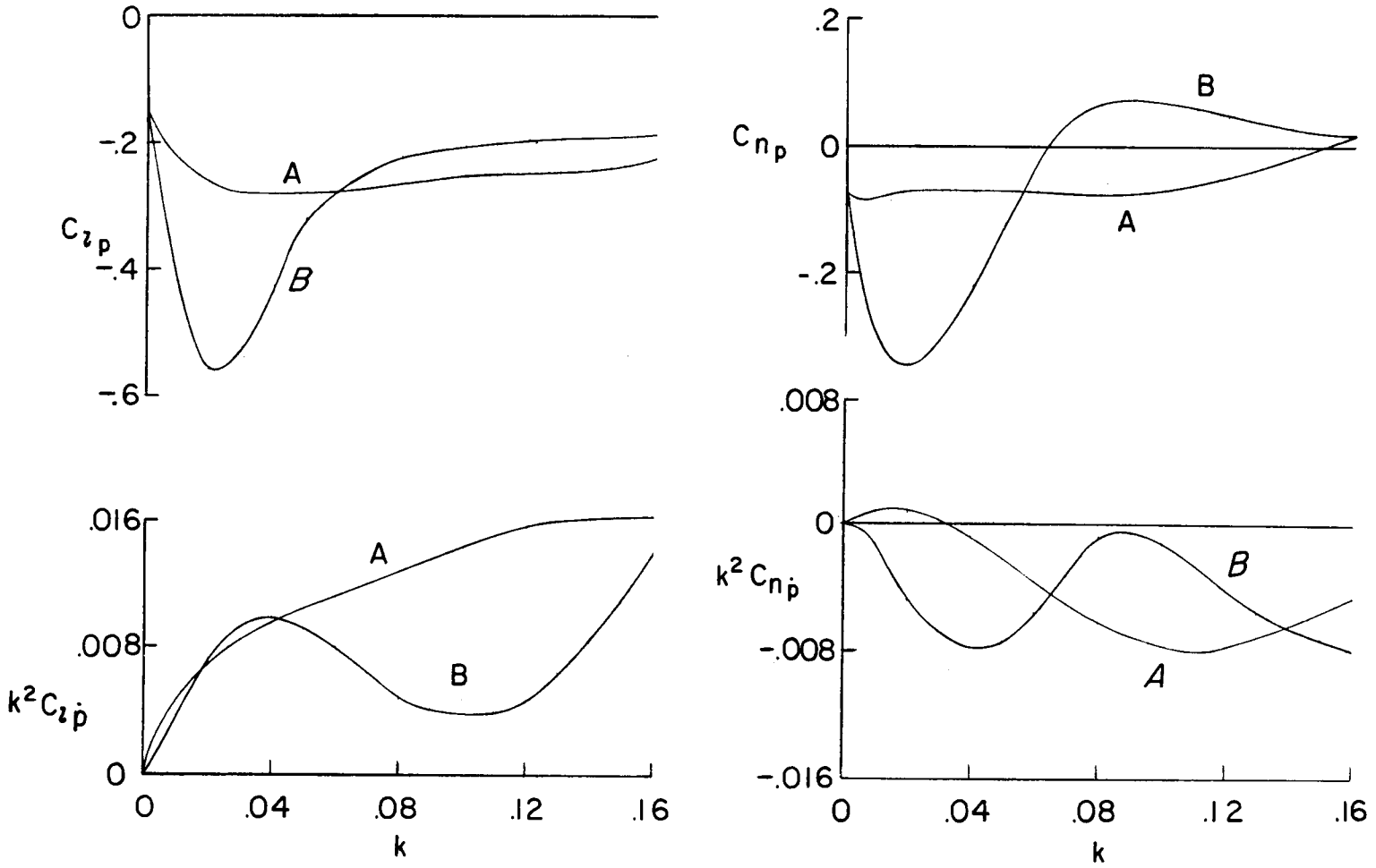

(b) Roll derivatives.

Figure 3.- Continued.

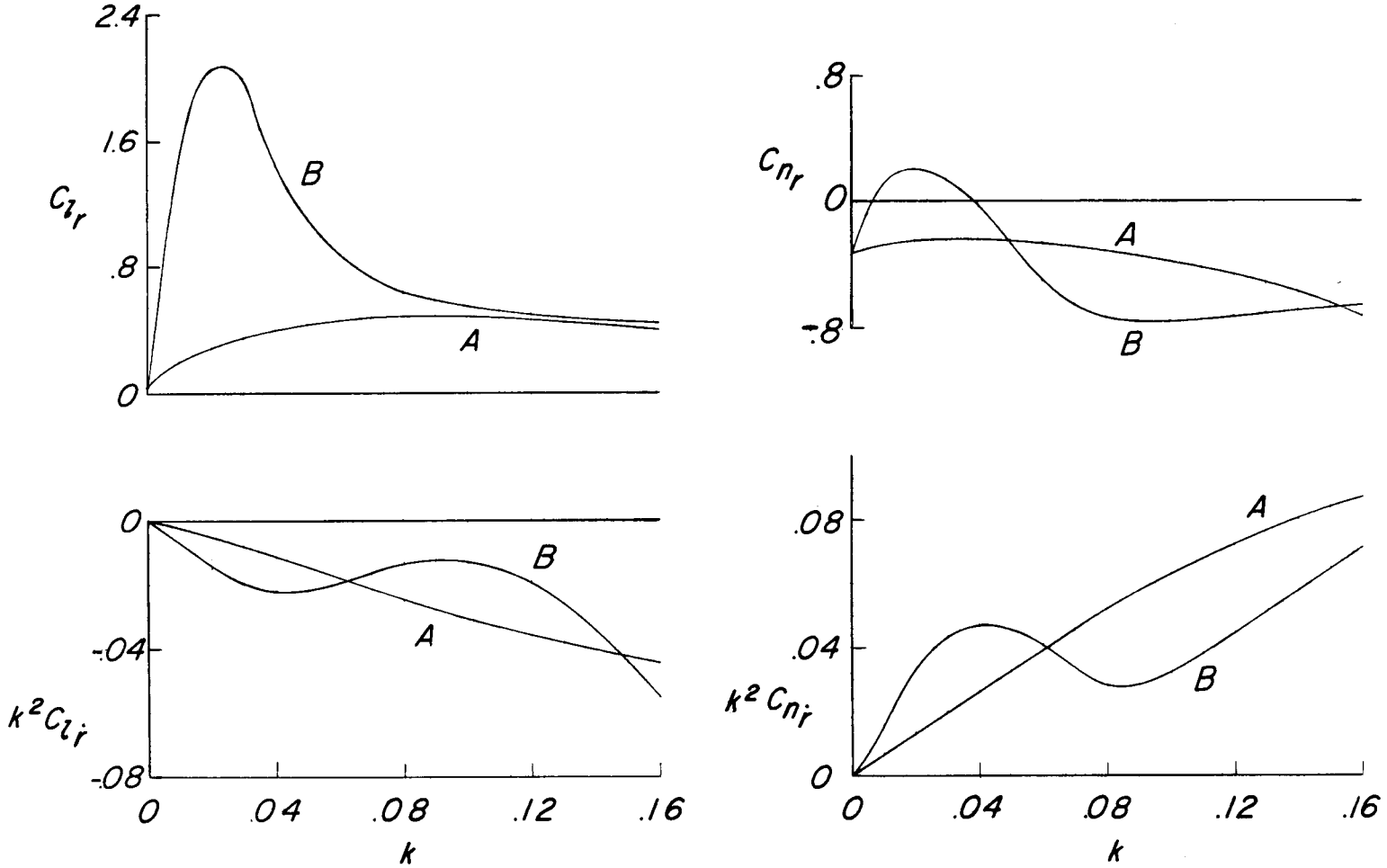

(c) Yaw derivatives.

Figure 3.- Concluded.

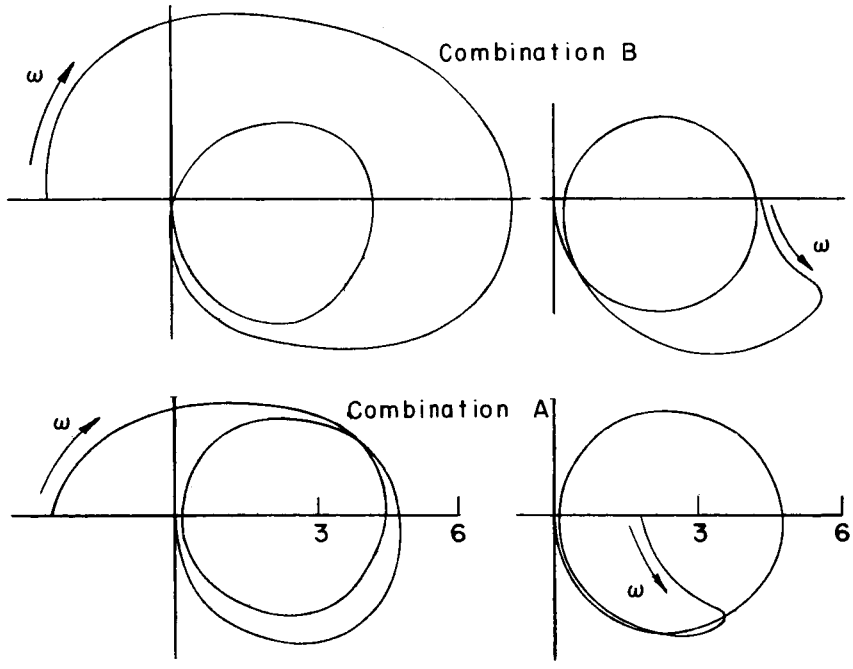

(a) Frequency-dependent stability derivatives.

(b) Dutch roll frequency-evaluated stability derivatives.

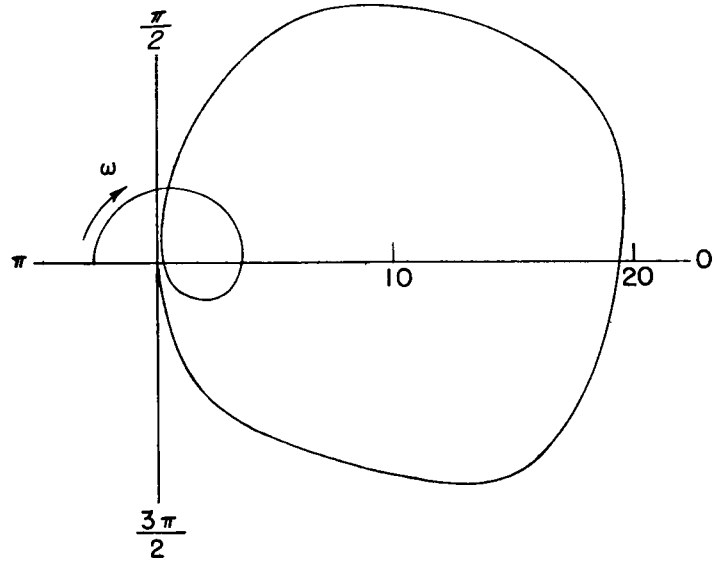

(c) Steady-state-evaluated stability derivatives.

Figure 4.- Polar diagrams of frequency response $\left[D\phi/C_l\right]$.

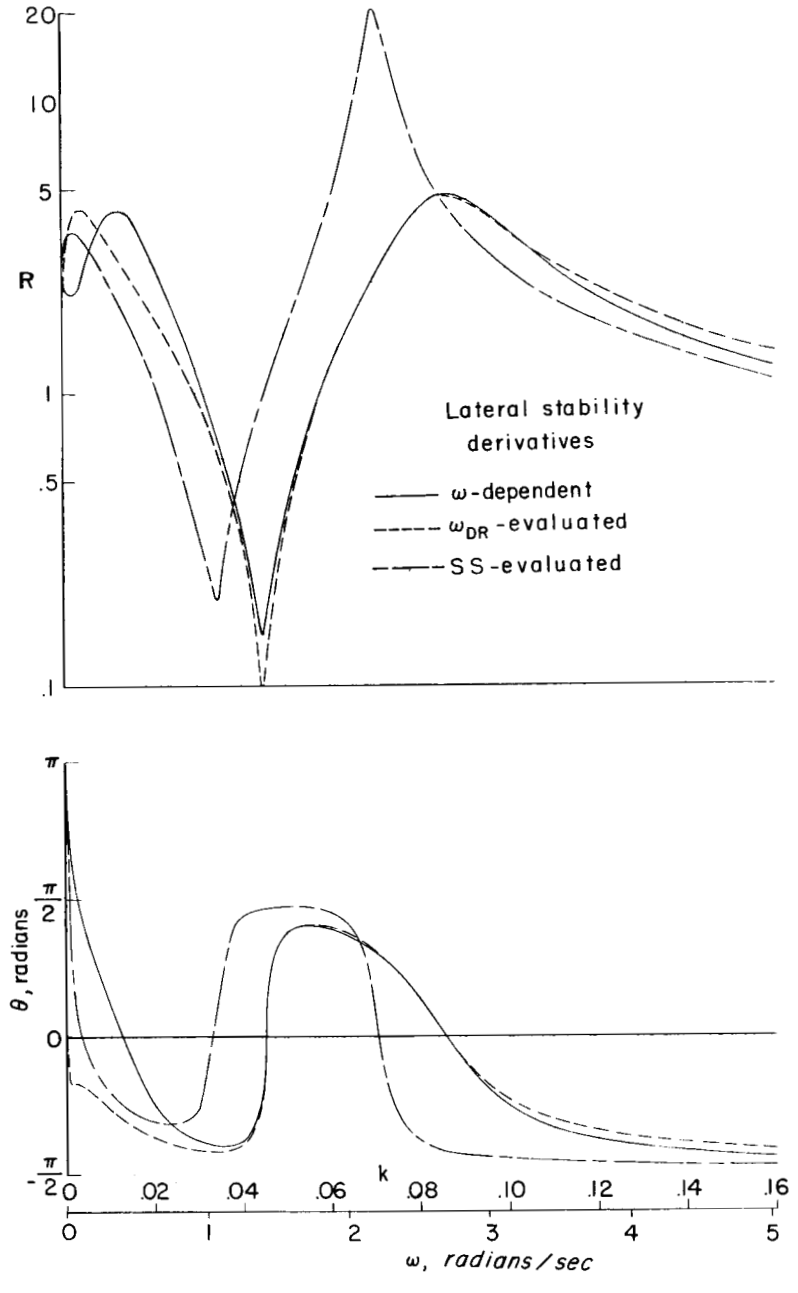

(a) $\left[\frac{D\phi}{C_l}\right]$.

Figure 5.- Frequency-response characteristics in roll and sideslip for frequency-dependent and constant stability derivatives. Combination A.

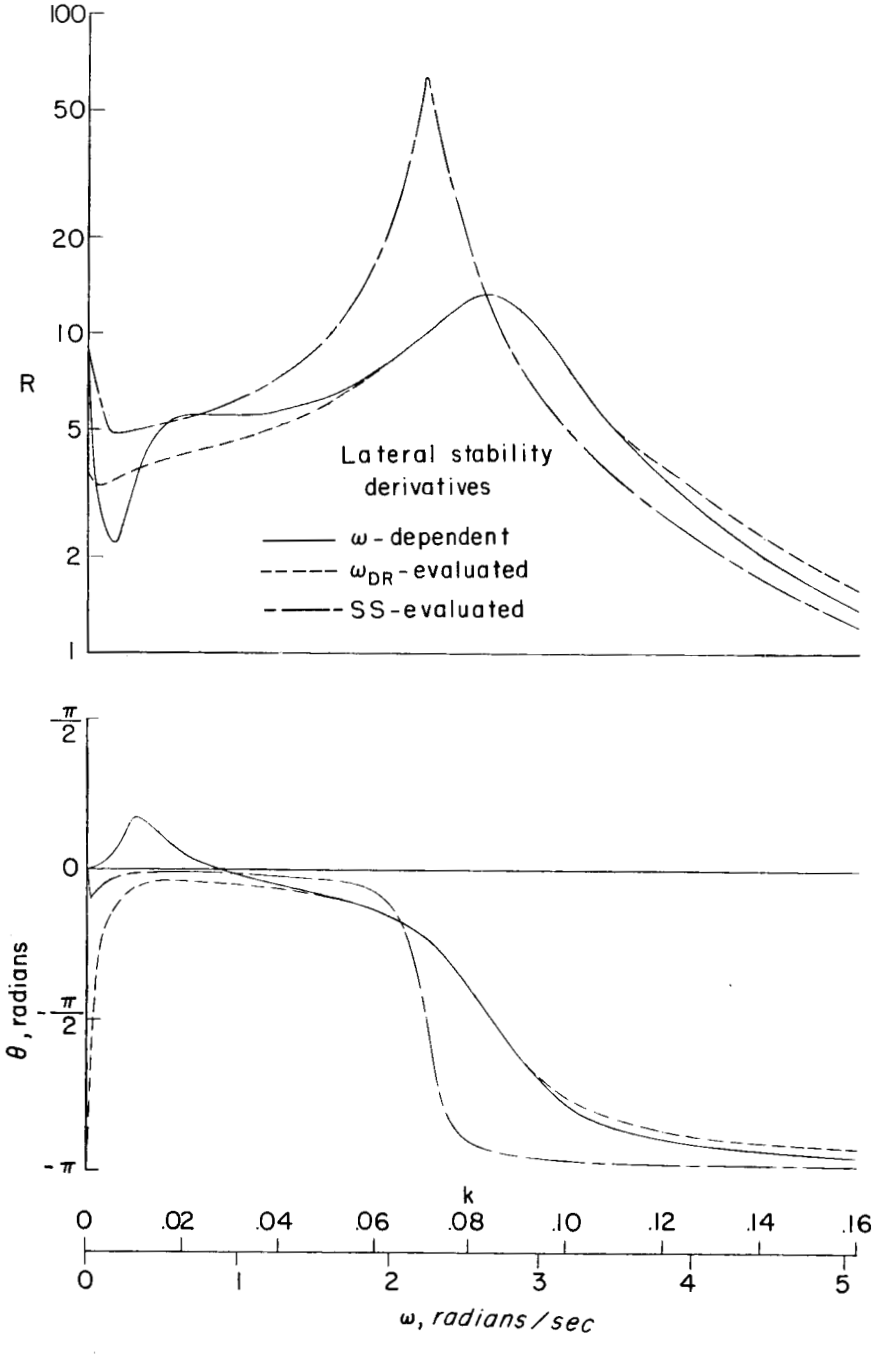

(b) $\left[\frac{\beta}{C_l}\right]$.

Figure 5.- Continued.

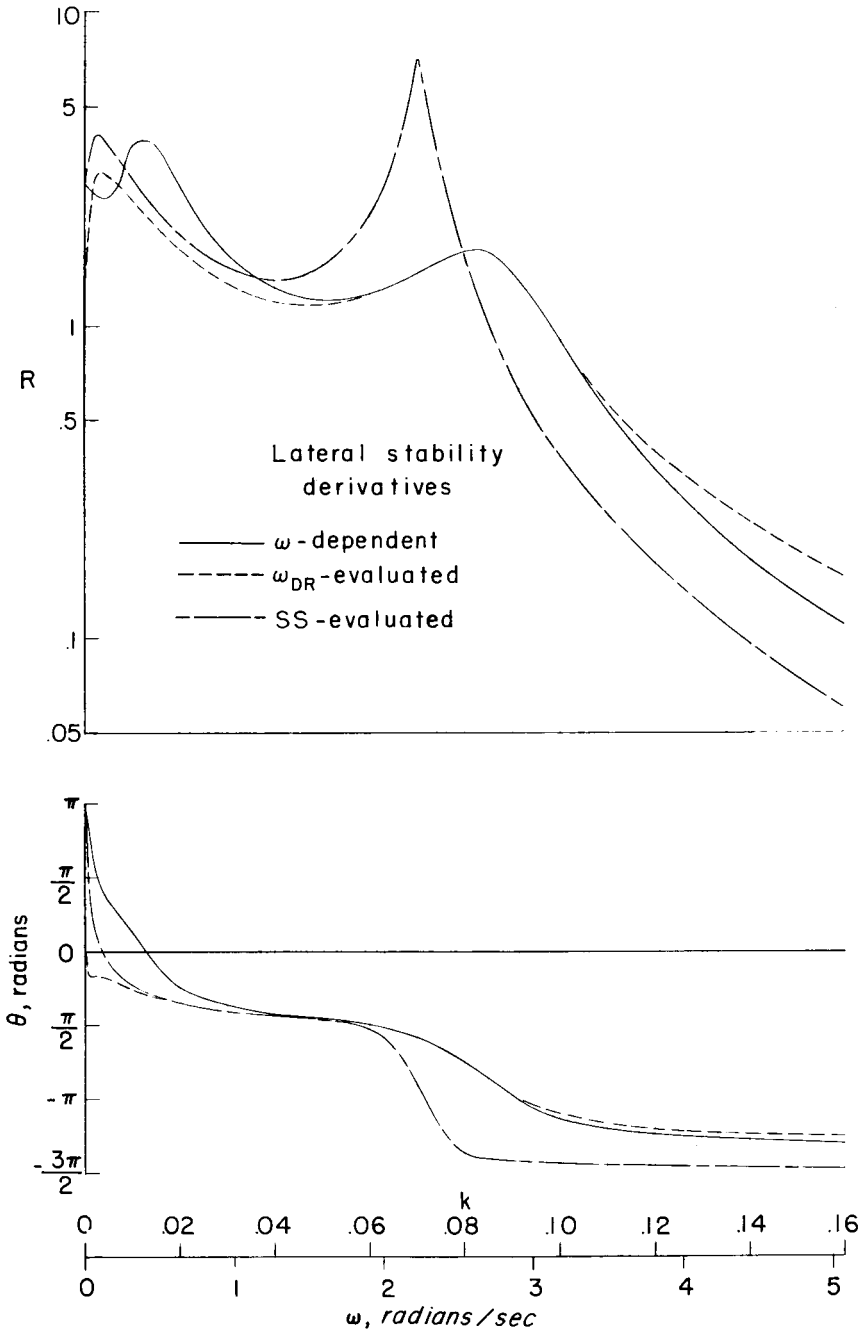

(c) $\left[\frac{D\phi}{C_n}\right]$.

Figure 5.- Continued.

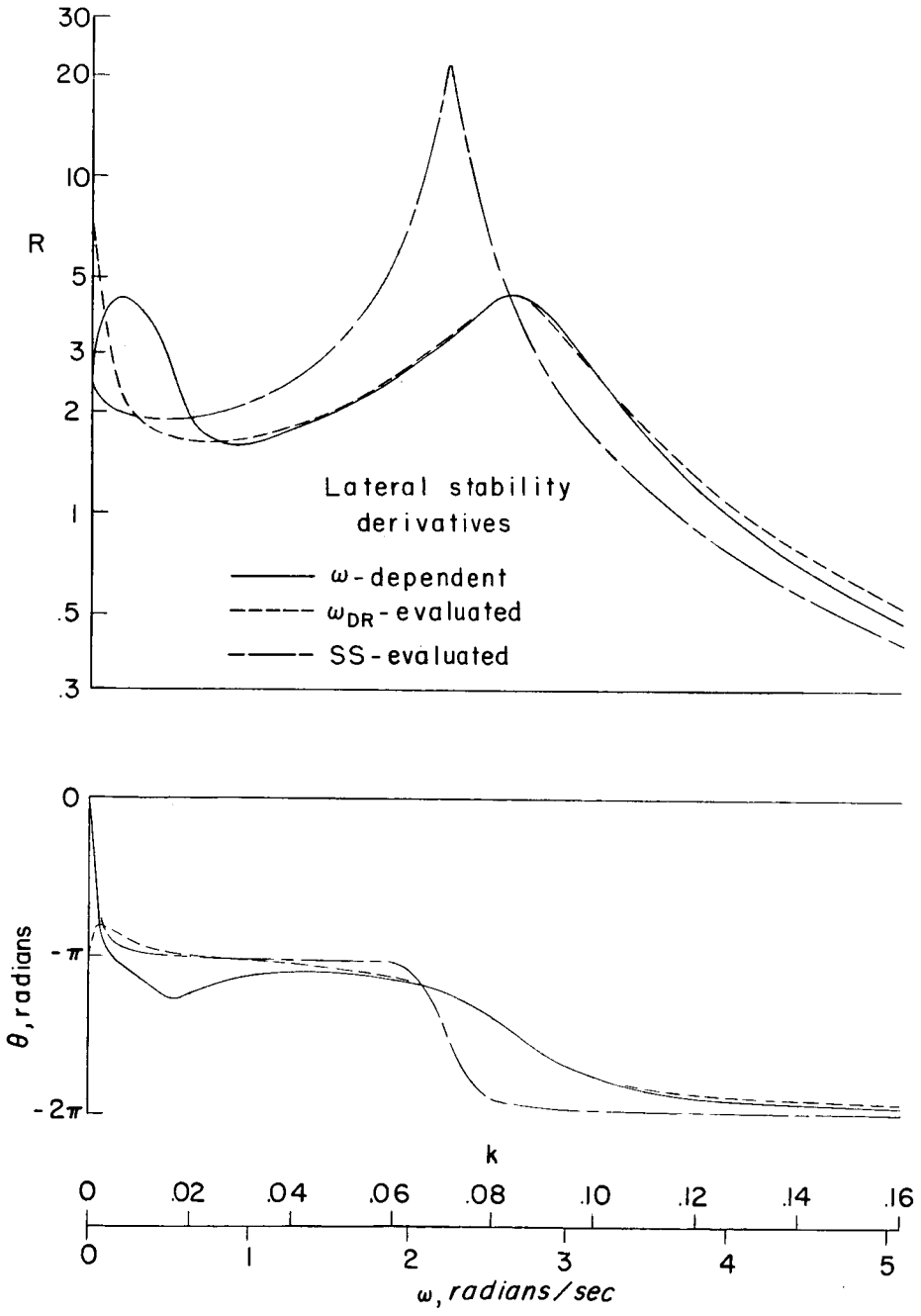

(d) $\left[\frac{\beta}{C_n}\right]$.

Figure 5.- Concluded.

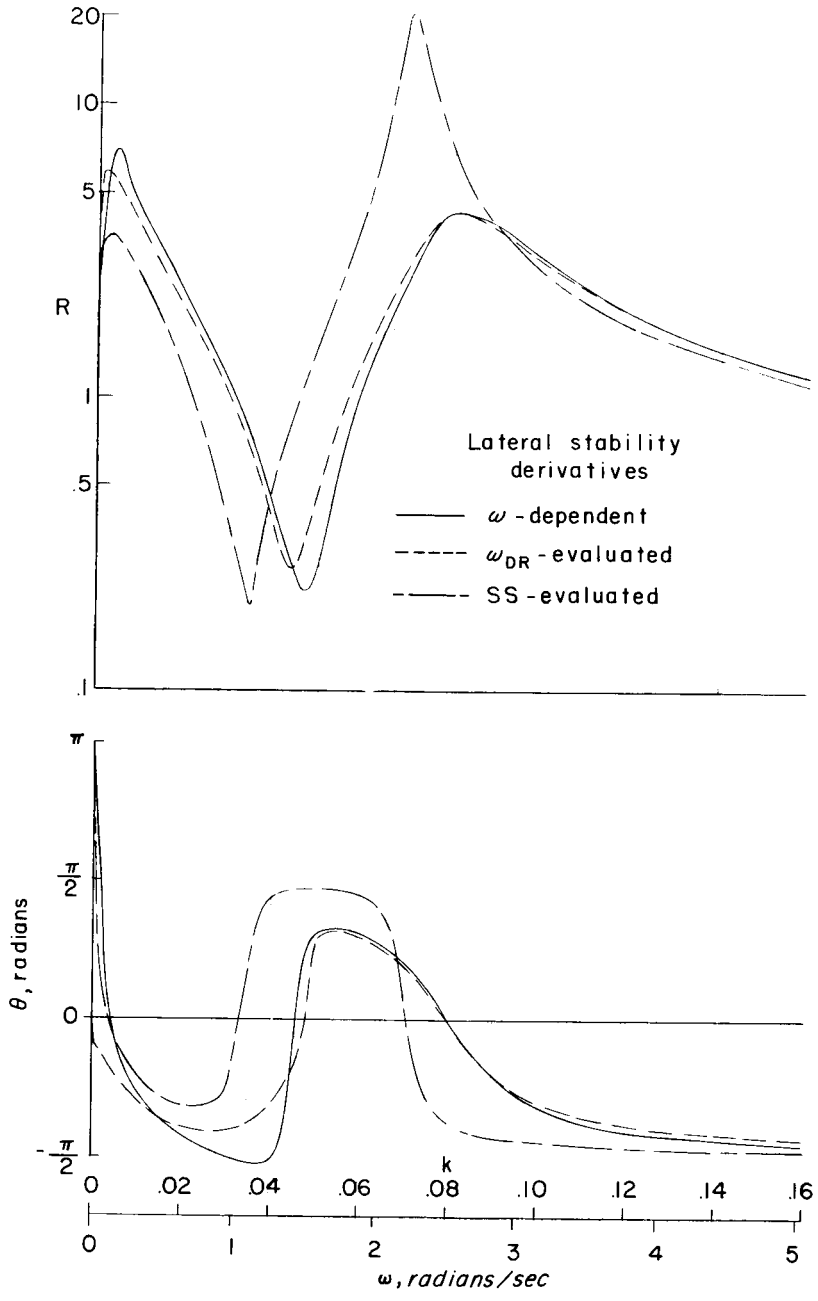

(a) $\left[\frac{D\phi}{C_l}\right]$.

Figure 6.- Frequency-response characteristics in roll and sideslip for frequency-dependent and constant stability derivatives. Combination B.

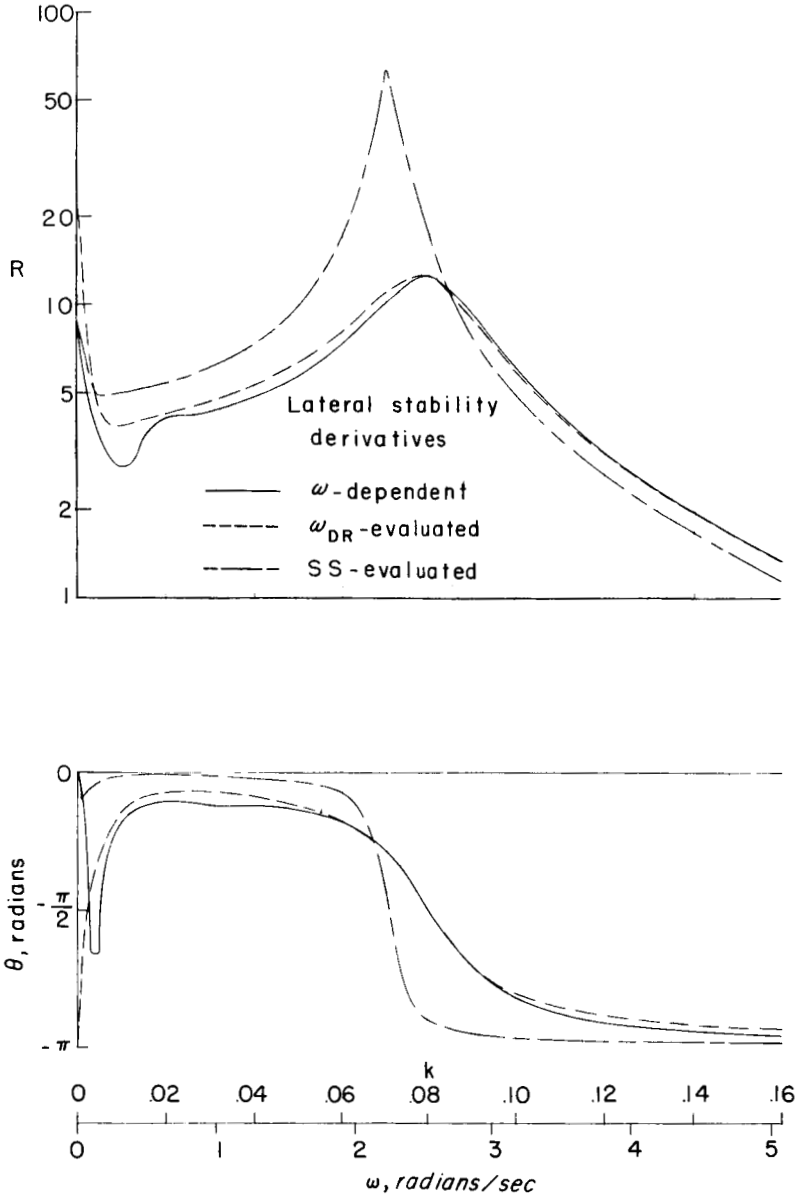

(b) $\left[\frac{\beta}{C_l}\right]$.

Figure 6.- Continued.

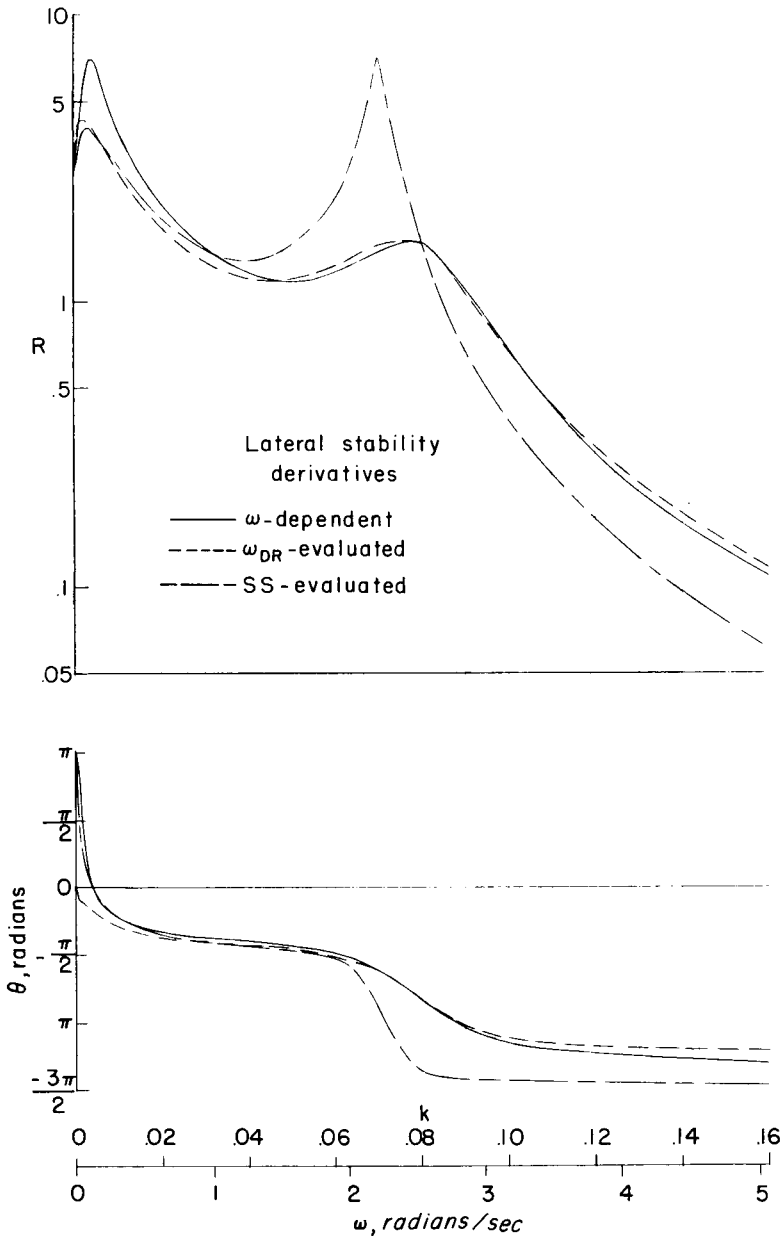

(c) $\left[\frac{D\phi}{C_n}\right]$.

Figure 6.- Continued.

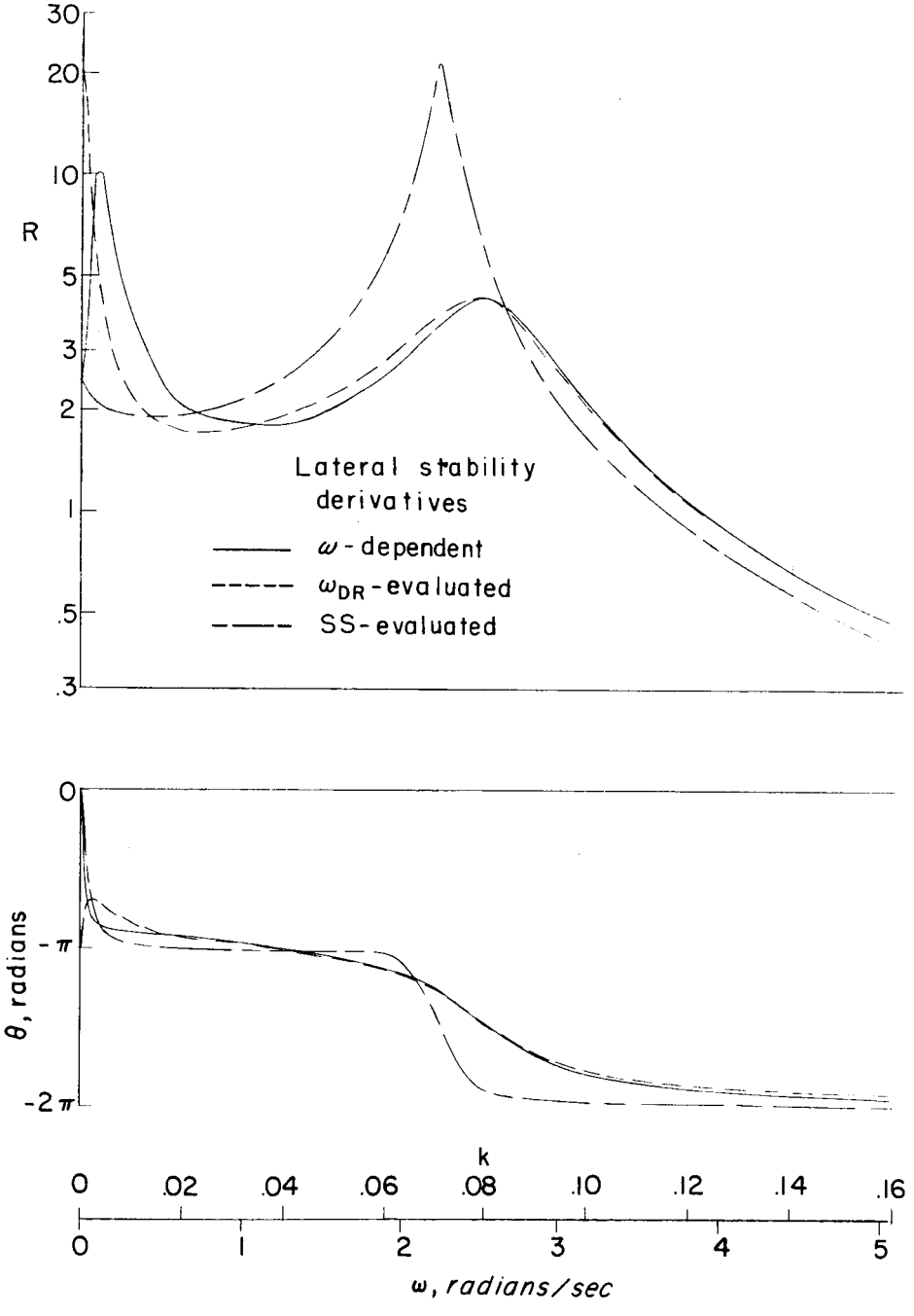

(d) $\left[\frac{\beta}{C_n}\right]$.

Figure 6.- Concluded.

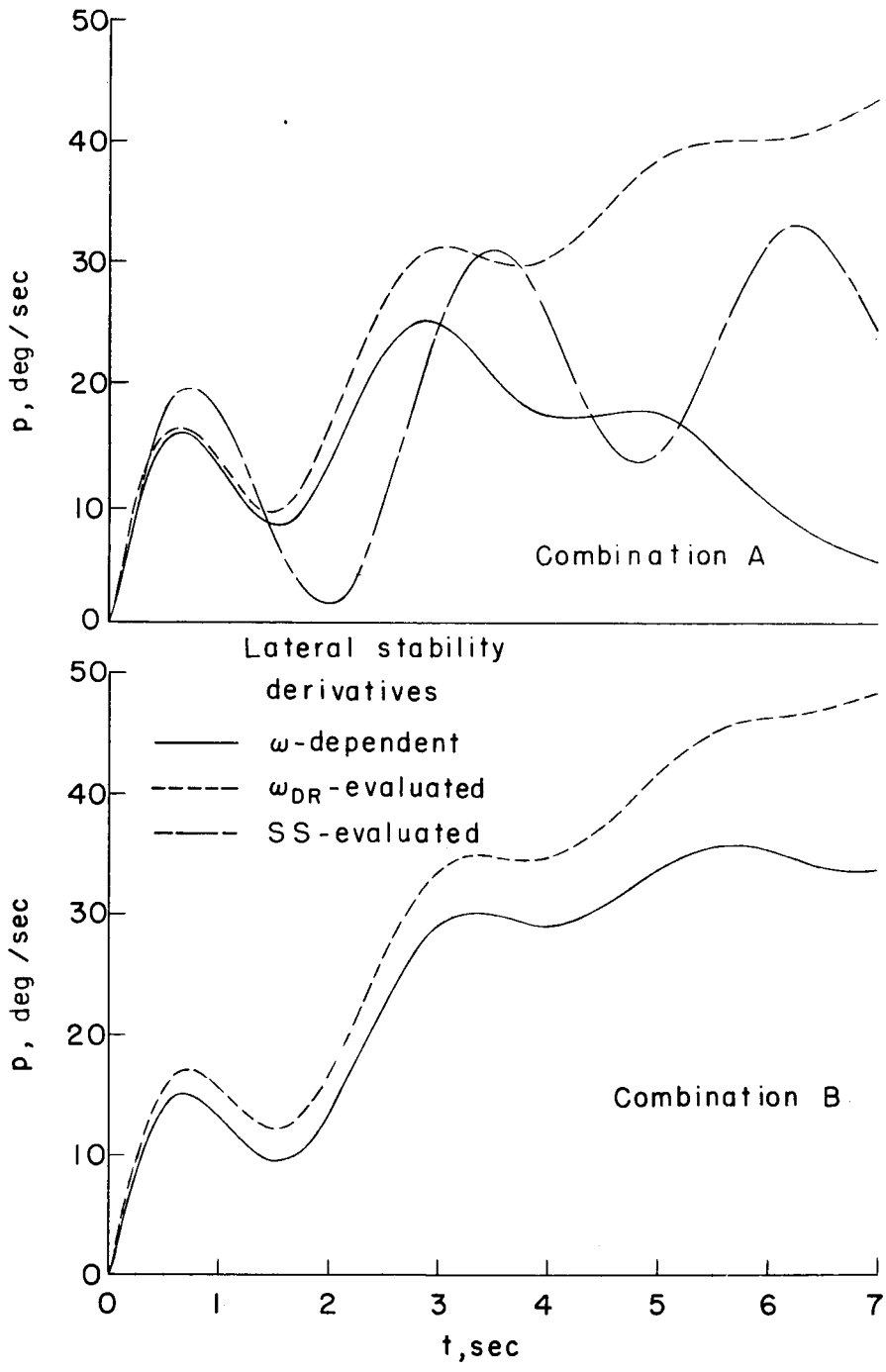

(a) Rolling velocity.

Figure 7.- Time histories of roll and sideslip motions to a step rolling-moment input. $C_l = 0.01$.

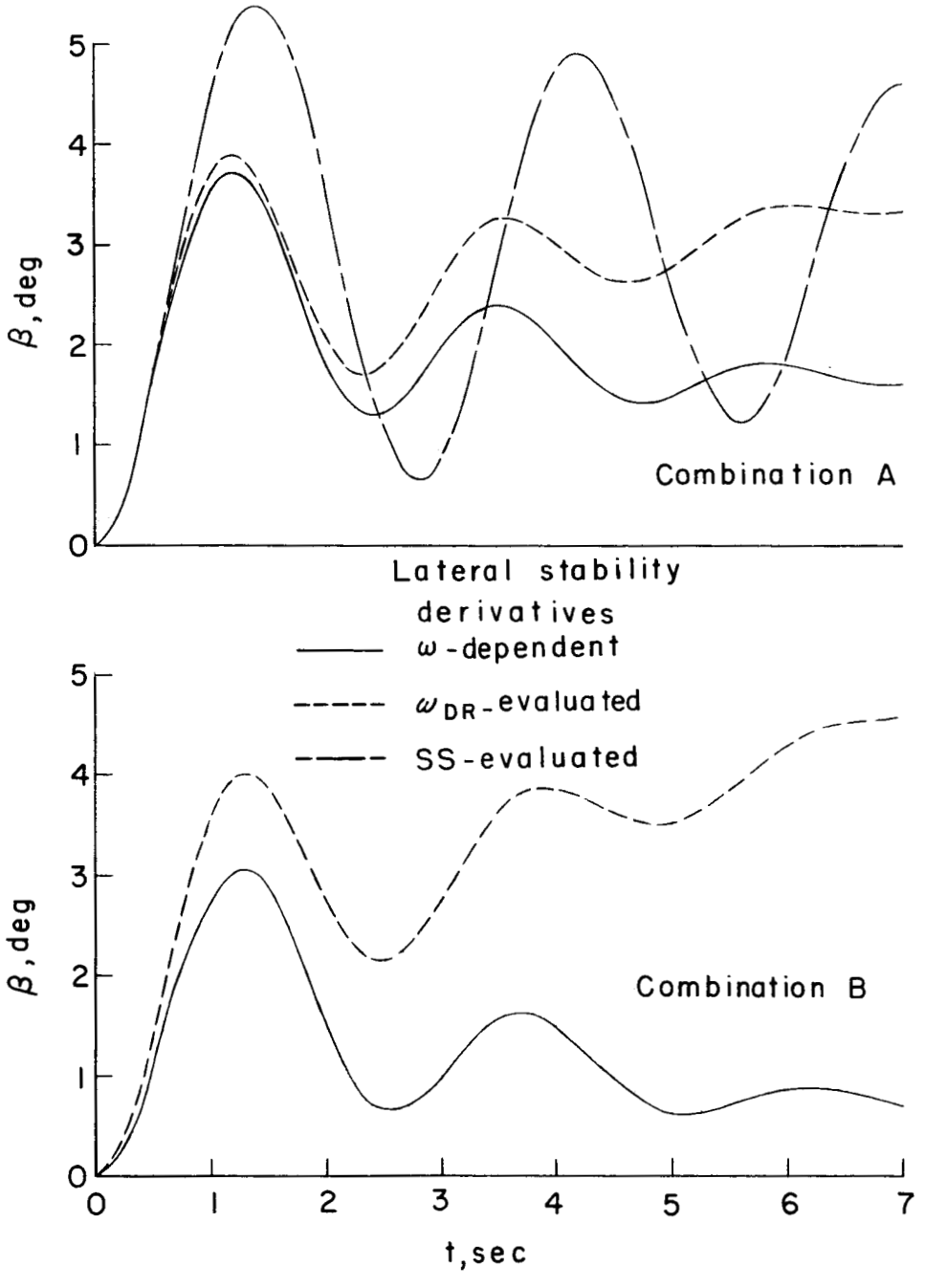

(b) Angle of sideslip.

Figure 7.- Concluded.

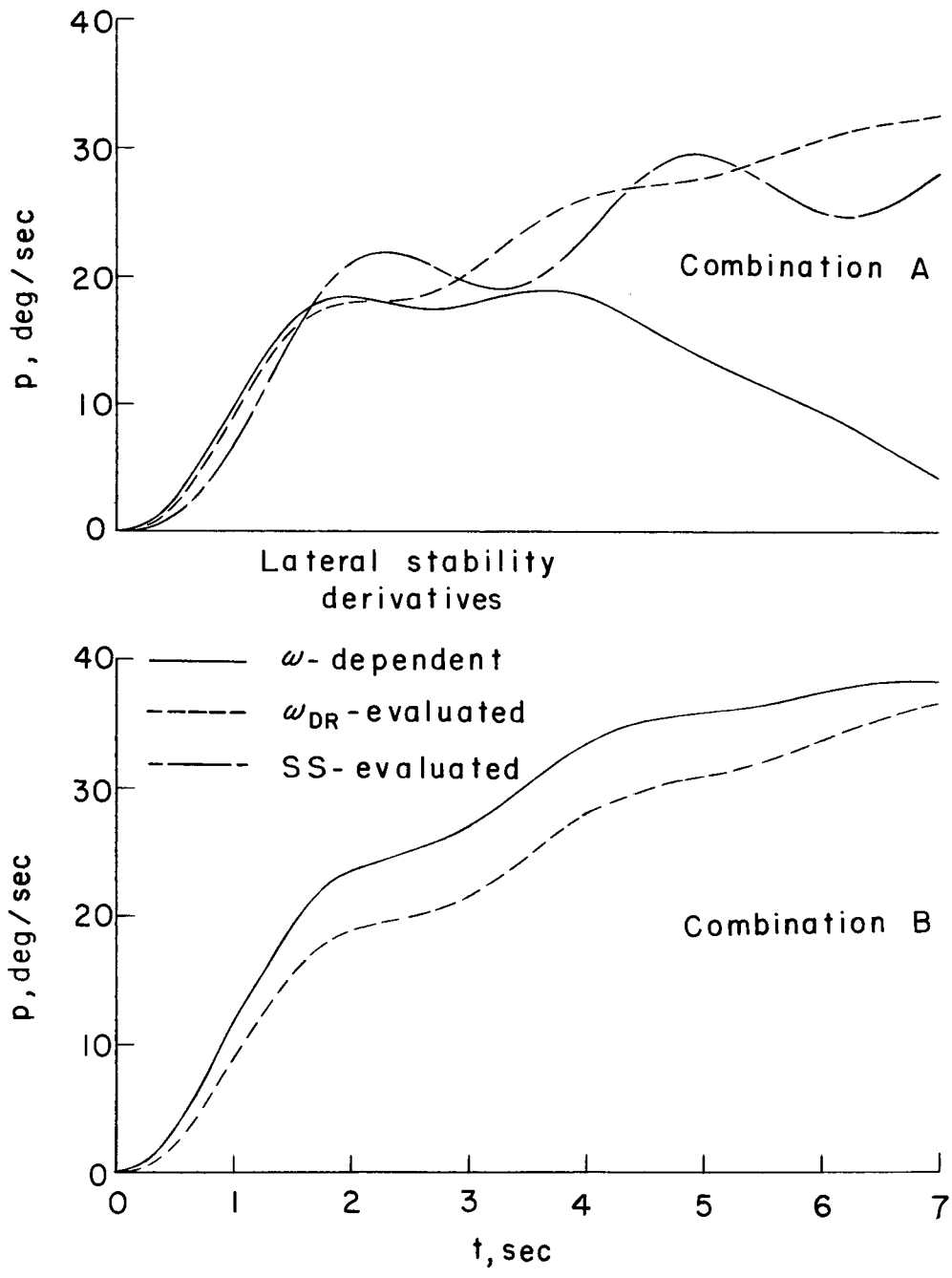

(a) Rolling velocity.

Figure 8.- Time histories of roll and sideslip motions to a step yawing-moment input. $C_n = 0.01$.

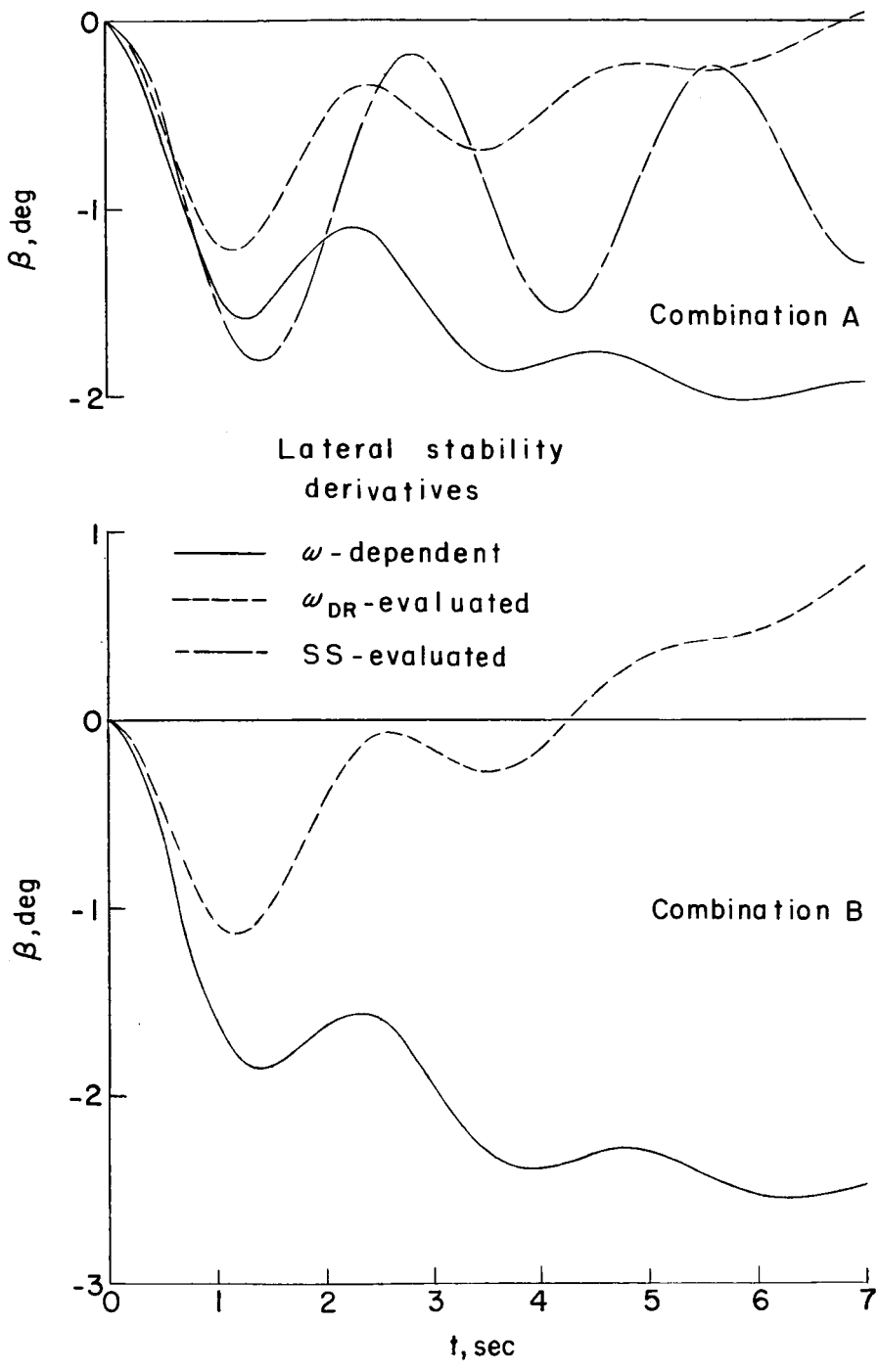

(b) Angle of sideslip.

Figure 8.- Concluded.

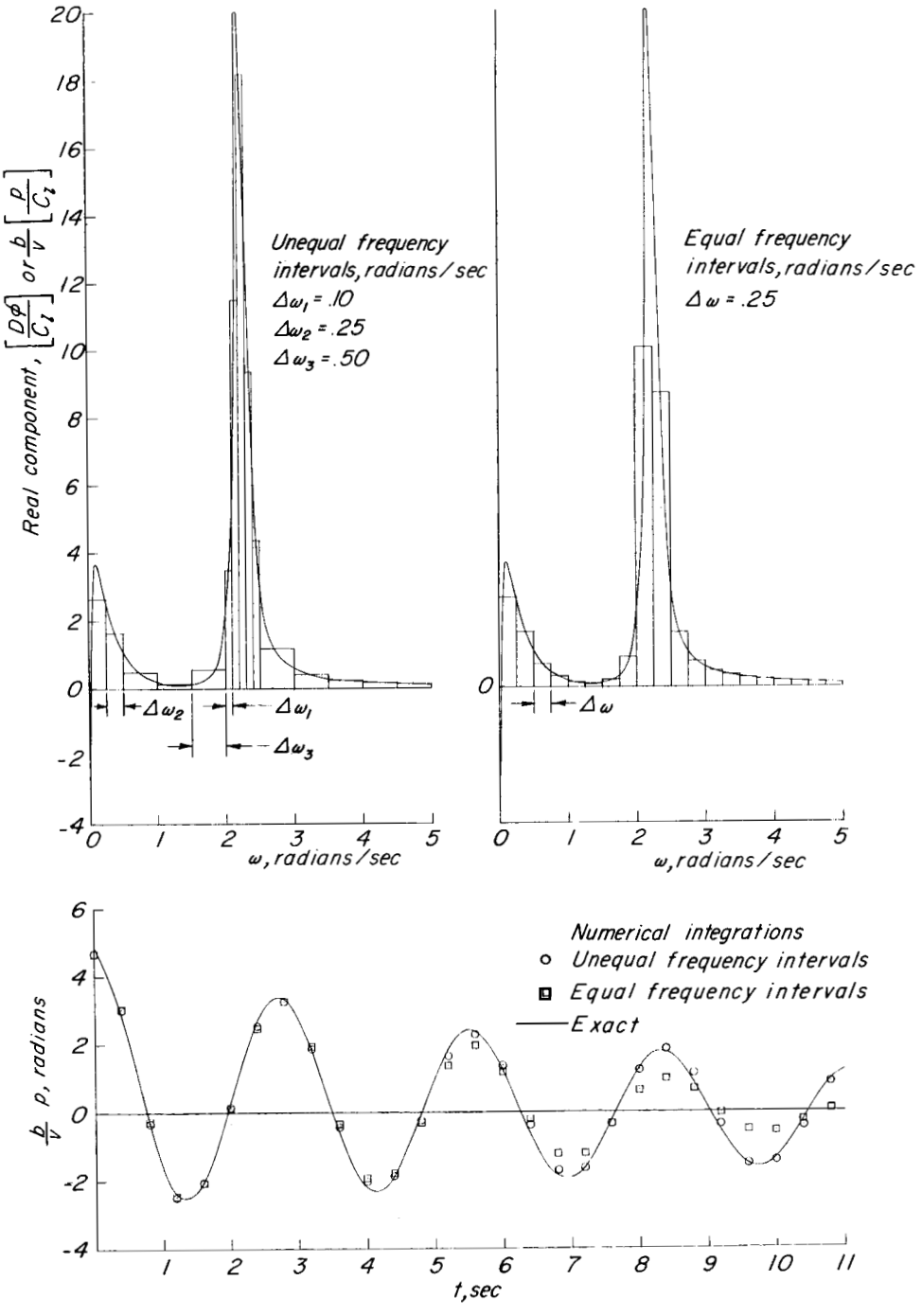

Figure 9.- Comparison of the responses to a unit impulse calculated from frequency-response data with the exact response for the illustrative problem of appendix B.

L-561